國立臺灣大學電機資訊學院電信工程學研究所

碩士論文

Graduate Institute of Communication Engineering

College of Electrical Engineering and Computer Science

National Taiwan University

Master's Thesis

一種適用於多重輸入輸出之正交時頻空間、正交時序多工及正交分頻多工系統的通道通用估測方法

A General Channel Estimation Method for MIMO OTFS, OTSM, and OFDM System

陳子齊

Zi-Qi Chen

指導教授：林茂昭 博士、李晃昌 博士

Advisor: Mao-Chao Lin, Ph.D, Huang-Chang Lee, Ph.D

中華民國 114 年 7 月

July, 2025

doi:10.6342/NTU202503398

國立臺灣大學碩士學位論文
口試委員會審定書
MASTER'S THESIS ACCEPTANCE CERTIFICATE
NATIONAL TAIWAN UNIVERSITY

（論文中文題目）(Chinese title of Master's Thesis)

一種適用於多重輸入輸出之正交時頻空間、正交時序多工及正交分頻多工系統的通道通用估測方法

（論文英文題目）(English title of Master's Thesis)

A General Channel Estimation Method for MIMO OTFS, OTSM, and OFDM System

本論文係 陳子齊 (姓名) r12942050 （學號）在國立臺灣大學電信工程學研究所完成之碩士學位論文，於民國 114 年 7 月 25 日承下列考試委員審查通過及口試及格，特此證明。

The undersigned, appointed by the Graduate Institute of Communication Engineering on 25 (date) 7 (month) 2025 (year) have examined a Master's Thesis entitled above presented by Chen, Zi-Qi (name) r12942050 (student ID) candidate and hereby certify that it is worthy of acceptance.

口試委員 Oral examination committee:

（指導教授 Advisor）

所長 Director:

誌謝

本論文能得以順利完成，首先我要衷心感謝我的恩師林茂昭教授與李晃昌教授。在我研究過程中，兩位教授不僅包容了我時常拖延的壞習慣，更在我迷惘與困頓時耐心地引導我前進。他們經常與我深入討論研究主題，提供寶貴的建議與明確的方向，使我能夠逐步釐清思路，完成論文。這份來自師長的信任與支持，是我能堅持走下去的重要力量。

同時，我也要感謝口試委員趙啟超教授、蘇育德教授與呂忠津教授，感謝他們撥冗參與本論文的審查，提出深刻且具啟發性的建議，讓本論文的內容更加完善與嚴謹。各位教授的專業意見，不僅豐富了本研究的深度，也讓我受益良多。

我還要感謝我的同學。在我們這一屆中，老師僅帶領兩位學生，因此我們之間建立了深厚的情誼與默契。正是因為彼此扶持、互相鼓勵，我們才能在壓力中成長、在挑戰中前行。這段並肩奮鬥的經歷，將成為我珍貴的回憶。

此外，我也要感謝實驗室的學長姐與學弟們。在這兩年的研究所生活中，雖然我們之間的交流並不頻繁，但每當我遇到困難時，總能感受到來自他們的熱心協助與支持。他們的存在，讓這段旅程不再孤單，也讓我學習到許多寶貴的經驗。

最後，我要深深感謝我的家人。在我攻讀研究所的期間，他們始終站在我身後，默默地提供生活上的照顧與情感上的支援。他們的包容與鼓勵，是我面對壓力與挑戰時最堅強的後盾。

回首這兩年的研究所時光，充滿挑戰也充滿驚喜。這段旅程不僅讓我累積了學術上的知識與能力，也讓我在人生的道路上獲得了成長。這些經歷將在我未來面對更多未知與困難時，成為我堅定前行的力量。

doi:10.6342/NTU202503398

中文摘要

本論文探討適用於多重輸入多重輸出之正交時頻空間、正交時序多工與正交分頻多工系統的通道估測方法。針對高速移動環境下通道估測與等化的挑戰，提出一種基於插值的導頻通道估測方法，結合區塊式最小均方誤差等化，能有效降低運算複雜度並維持優異的偵測性能。

此外，本研究針對多重輸入多重輸出系統提出一種僅需單一導頻的通道估測架構，利用曲線擬合與符號交替技術，有效降低導頻與保護間隔所需的開銷。透過一階、二階及三階的曲線擬合法，分析其在不同移動速度下的估測準確性，並提出多種修正策略以改善高速移動時的估測誤差。

模擬結果顯示，所提出的方法在維持良好誤比特率與均方誤差表現的同時，亦能有效降低系統的導頻開銷，特別是在中低速移動環境下展現出顯著優勢。

關鍵字：多重輸入多重輸出、正交時頻空間、正交時序多工、通道估測、導頻設計、曲線擬合

doi:10.6342/NTU202503398

英文摘要

This thesis investigates channel estimation techniques for Multiple-Input Multiple-Output (MIMO) systems based on Orthogonal Time Frequency Space (OTFS), Orthogonal Time Sequency Modulation (OTSM), and Orthogonal Frequency Division Multiplexing (OFDM). To address the challenges posed by rapidly time-varying channels in high-mobility scenarios, an interpolation-based pilot-assisted channel estimation method combined with blockwise Minimum Mean Square Error (MMSE) equalization is proposed, achieving reduced computational complexity while maintaining reliable detection performance.

Furthermore, a novel pilot-efficient channel estimation framework for MIMO OTFS/OTSM systems is developed, employing curve fitting and sign-alternating schemes to mitigate pilot contamination and reduce guard interval overhead. First-order, second-order, and third-order curve fitting methods are explored, and various refinement strategies are proposed to enhance estimation accuracy under high Doppler conditions.

Simulation results confirm that the proposed methods achieve favorable Bit Error Rate (BER) and Normalized Mean Square Error (NMSE) performance while significantly reducing pilot overhead, particularly in low to moderate mobility scenarios.

Key Words: MIMO, OTFS, OTSM, Channel Estimation, Pilot Design, Curve Fitting

doi:10.6342/NTU202503398

目次

doi:10.6342/NTU202503398

doi:10.6342/NTU202503398

圖次

doi:10.6342/NTU202503398

doi:10.6342/NTU202503398

表次

第一章　Introduction

1.1 Motivation

The rapid advancement of wireless communication systems has driven growing demands for higher data rates, robust connectivity, and reliable performance across diverse channel conditions. Conventional multicarrier modulation schemes, particularly Orthogonal Frequency Division Multiplexing (OFDM), have been widely adopted owing to their efficiency in combating multipath fading and enabling high spectral efficiency. However, OFDM systems suffer significant performance degradation in high-mobility environments, mainly because the channel quasi-static assumption no longer holds, leading to inter-carrier interference (ICI) induced by Doppler effects.

To address these limitations, advanced modulation schemes have been proposed, including Orthogonal Time Frequency Space (OTFS) [1], [7] and Orthogonal Time Sequency Modulation (OTSM) [3], [4]. These approaches exploit the sparsity of wireless channels in alternative domains — such as delay-Doppler or delay-sequency — to enhance resilience against channel dynamics and improve symbol detection in rapidly varying environments.

Despite their promising theoretical advantages, practical implementation of OTFS and OTSM systems introduces significant challenges, particularly in the areas of channel estimation and equalization [4], [5], [8], [9], [10], [11], [12], [13], [14], [15], [16]. The complexity of high-dimensional signal processing, the impact of Doppler spread, and the need for efficient detection algorithms highlight the necessity for novel methods that ensure performance gains without incurring prohibitive computational costs. Moreover, extending these techniques to multiple-input multiple-output (MIMO) configurations further amplify these challenges due to the inherent increase in system

doi:10.6342/NTU202503398

dimensionality.

1.2 Contribution

This thesis investigates advanced signal processing techniques for OTFS and OTSM systems with an emphasis on improving channel estimation and equalization performance in high-mobility scenarios. A key contribution of this thesis is the development of a pilot-efficient channel estimation method for MIMO OTFS/OTSM systems. Unlike conventional multi-pilot designs that introduce significant pilot and guard interval overhead, the proposed method employs a single pilot combined with curve fitting and sign-alternating techniques. This approach significantly reduces the overhead while maintaining comparable BER and NMSE performance, particularly in low to moderate mobility scenarios. The method demonstrates that even under lower mobility conditions, similar estimation accuracy can be achieved with substantially lower resource consumption.

1.3 Structure of Thesis

This thesis is structured as follows:

Chapter 2 – Background Knowledge: Provides an overview of fundamental concepts in OFDM, OTFS, and OTSM systems, elaborating on their modulation principles, system architectures, and underlying mathematical models. It also introduces the channel model used throughout the study and reviews the conventional MMSE detection scheme.

Chapter 3 – Channel Estimation Methods for MIMO Systems: Extends the discussion to MIMO configurations, presenting both traditional and proposed pilot-based channel estimation techniques. The chapter details the design considerations, mathematical

doi:10.6342/NTU202503398

derivations, and modifications required for effective channel estimation in MIMO OTFS/OTSM systems.

Chapter 4 – Numerical Results: Presents simulation results validating the theoretical analysis and proposed methods. The chapter includes comprehensive performance evaluations under different Doppler shifts and system configurations, offering insights into the practical implications of the proposed solutions.

Chapter 5 – Conclusion and Future Work: Summarizes the key findings of this thesis and highlights the effectiveness of the proposed single-pilot MIMO channel estimation method. The chapter also outlines potential directions for future research, including extensions to higher-order MIMO systems and adaptive estimation under diverse mobility conditions.

doi:10.6342/NTU202503398

第二章　Background Knowledge

2.1　OFDM System

Orthogonal Frequency Division Multiplexing (OFDM) is a widely adopted multicarrier modulation technique that divides the available spectrum into multiple orthogonal subcarriers. Each subcarrier carries a low data-rate stream, allowing efficient utilization of bandwidth and robustness against multipath fading. The orthogonality between subcarriers minimizes inter-carrier interference (ICI) under ideal synchronization and channel conditions.

In conventional wireless channels, multipath propagation causes time dispersion, leading to inter-symbol interference (ISI), which degrades system performance. OFDM mitigates this problem by employing a cyclic prefix (CP) that converts linear convolution with the channel into circular convolution, thereby preserving subcarrier orthogonality in frequency-selective fading environments.

A typical OFDM system structure is illustrated in Figure 2.1.

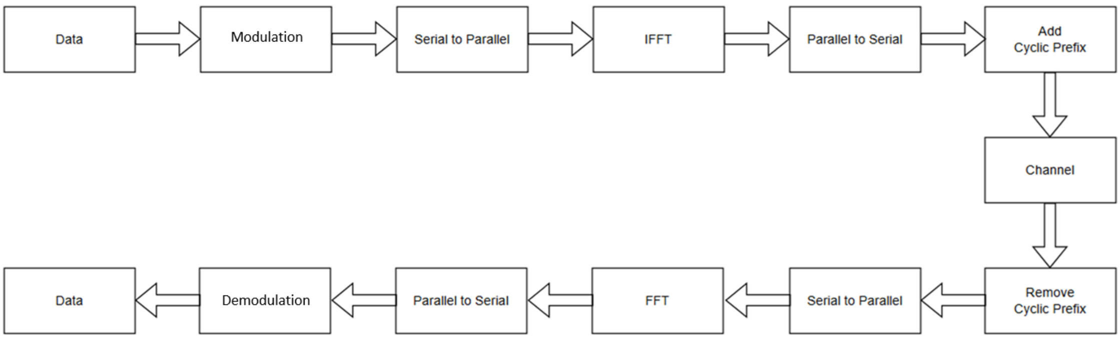

Figure 2.1 Typical OFDM System Structure

However, OFDM exhibits limitations under high-mobility scenarios. The assumption of quasi-static channels during an OFDM symbol period breaks down under significant Doppler shifts. The time-variation within an OFDM symbol duration leads to a breakdown in subcarrier orthogonality and results in Doppler-induced ICI. This

doi:10.6342/NTU202503398

degradation significantly impacts the symbol detection performance, especially in vehicular or high-speed railway environments where the channel coherence time is short.

To enhance performance in Doppler-dominant channels, various equalization and estimation strategies have been proposed, however, mitigating ICI remains a significant challenge. This challenge has motivated the exploration of alternative modulation schemes — such as OTFS and OTSM — that exploit channel sparsity in domains like delay-Doppler or delay-sequency.

2.2 OTFS System

Orthogonal Time Frequency Space (OTFS) modulation is a two-dimensional modulation scheme that maps information symbols into the delay–Doppler (DD) domain rather than the conventional time–frequency (TF) domain. OTFS leverages the quasi-static and sparse characteristics of wireless channels in the DD domain, offering improved resilience to both multipath delay spread and Doppler-induced time variations [1], [7].

Assume for an OTFS frame, we have a bandwidth of B_{OTFS} and a time duration of T_{OTFS}, defined in the TF domain. The bandwidth B_{OTFS} is divided into M subcarriers with subcarrier spacing $\Delta f = \frac{B_{OTFS}}{M}$, and the time duration T_{OTFS} is divided into N time slot with slot duration $T = \frac{T_{OTFS}}{N}$, where $T \cdot \Delta f = 1$.

At the transmitter, we assume $X_{DD}[l, k]$ denote the complex information symbols on the DD domain, where $l \in \{0,1, \dots, M-1\}$, $k \in \{0,1, \dots, N-1\}$ denoting the delay index and the Doppler index.

After the modulation, we use the inverse Symplectic Finite Fourier Transform

doi:10.6342/NTU202503398

(ISFFT) to convert the DD-domain symbols into the TF-domain samples.

$$X_{TF}[m,n] = \frac{1}{\sqrt{MN}} \sum_{k=0}^{N-1} \sum_{l=0}^{M-1} X_{DD}[l,k] e^{j2\pi\left(\frac{nk}{N}-\frac{ml}{M}\right)}. \tag{2.1}$$

, where $m \in \{0,1,\dots,M-1\}$, $n \in \{0,1,\dots,N-1\}$ denoting the subcarrier index and the time slot index.

The Heisenberg Transform is then applied to map these TF samples onto a continuous-time transmit signal using a pulse shaping filter $g_{tx}(t)$.

$$s(t) = \sum_{n=0}^{N-1} \sum_{m=0}^{M-1} X_{TF}[m,n] g_{tx}(t-nT) e^{j2\pi m\Delta f(t-nT)}. \tag{2.2}$$

At the receiver, we assume the received continuous-time signal is $r(t)$.

First, we will do the Wigner Transform to map the continuous-time signal onto TF samples with a pulse shaping filter $g_{rx}(t)$.

$$Y_{TF}[m,n] = \int g_{rx}^{*}(t-nT) r(t) e^{-j2\pi m\Delta f(t-nT)} dt. \tag{2.3}$$

Then, we use the Symplectic Finite Fourier Transform (SFFT) to convert the TF-domain samples into the DD-domain symbols.

$$Y_{DD}[l,k] = \frac{1}{\sqrt{MN}} \sum_{n=0}^{N-1} \sum_{m=0}^{M-1} Y_{TF}[m,n] e^{-j2\pi\left(\frac{nk}{N}-\frac{ml}{M}\right)}. \tag{2.4}$$

A typical system structure of OTFS is shown in Figure 2.2

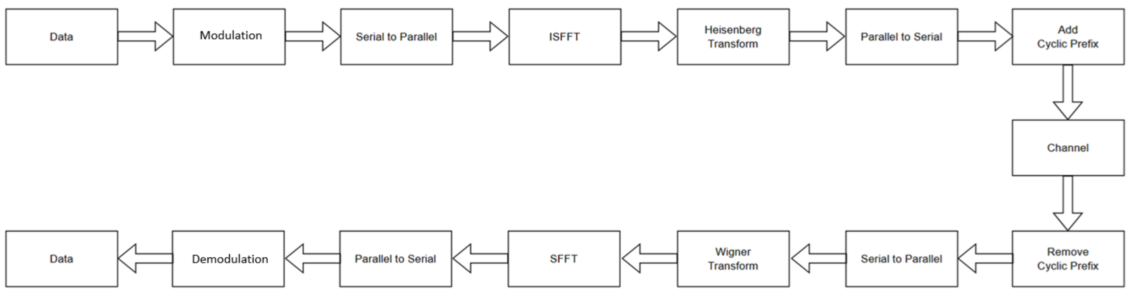

Figure 2.2 Typical OTFS System Structure

doi:10.6342/NTU202503398

The equations above can be written into the matrix form shown below.

N-point FFT Matrix: F_N.

ISFFT:

$$X_{TF} = F_M X_{DD} F_N^H. \tag{2.5}$$

Heisenberg Transform:

$$S = G_{tx} F_M^H X_{TF} = G_{tx} F_M^H F_M X_{DD} F_N^H = G_{tx} X_{DD} F_N^H. \tag{2.6}$$

The transmitted pulse shaping filter matrix:

$$G_{tx} = diag\left(g_{tx}(0), g_{tx}\left(\frac{T}{M}\right), \dots, g_{tx}\left((M-1)\frac{T}{M}\right)\right). \tag{2.7}$$

The transmitted signal: $s = vec(S)$.

The received signal: $r = vec^{-1}(R)$.

Wigner Transform:

$$Y_{TF} = F_M G_{rx} R. \tag{2.8}$$

The received pulse shaping filter matrix:

$$G_{rx} = diag\left(g_{rx}(0), g_{rx}\left(\frac{T}{M}\right), \dots, g_{rx}\left((M-1)\frac{T}{M}\right)\right). \tag{2.9}$$

SFFT:

$$Y_{DD} = F_M^H Y_{TF} F_N = F_M^H F_M G_{rx} R F_N = G_{rx} R F_N. \tag{2.10}$$

From the matrix expressions above, we can find that the M-point IFFT matrix and FFT matrix in the Heisenberg Transform and SFFT eliminated with each other. With this discovery, we can reduce the computation both at the transmitter and the receiver.

At the transmitter, we can do N point IFFT to each row on the the complex information symbols on the DD domain; at the receiver, we can do N point FFT to each row on the folded received signal.

doi:10.6342/NTU202503398

Rectangular waveforms are preferable for both transmitted and received pulse shaping filters, as they result in a unitary pulse shaping filter matrix [2].

2.3 OTSM System

Orthogonal Time Sequency Modulation (OTSM) is a recently proposed multicarrier modulation technique that operates in the delay–sequency domain, offering an alternative to both traditional OFDM and OTFS [3], [4]. The core idea of OTSM is to substitute the Fourier Transform in OTFS with the Walsh–Hadamard Transform (WHT), enabling a real-valued, addition-only implementation. This significantly reduces computational complexity while maintaining favorable performance in time-varying and multipath-rich wireless environments.

OTSM employs sequency-ordered Walsh functions, which are a set of orthogonal, piecewise constant functions that take values of ±1 over dyadic intervals [6].
Unlike frequency, sequency refers to the number of zero crossings per unit interval, providing a discrete and deterministic alternative to sinusoids in Fourier transforms.

Over the interval of $0 \leq \lambda < 1$, the Walsh functions are denoted by $W(n,\lambda)$, where $n = 0,1,\ldots,N-1$ denoting the sequency index.

For example, if $N = 8$, the sequency-ordered Walsh functions can be written as:

$W(0,\lambda) = [1,1,1,1,1,1,1,1]$,

$W(1,\lambda) = [1,1,1,1,-1,-1,-1,-1]$,

$W(2,\lambda) = [1,1,-1,-1,-1,-1,1,1]$,

$W(3,\lambda) = [1,1,-1,-1,1,1,-1,-1]$,

$W(4,\lambda) = [1,-1,-1,1,1,-1,-1,1]$,

$W(5,\lambda) = [1,-1,-1,1,-1,1,1,-1]$,

$W(6,\lambda) = [1,-1,1,-1,-1,1,-1,1]$,

doi:10.6342/NTU202503398

$W(7,\lambda) = [1,-1,1,-1,1,-1,1,-1]$,

Figure 2.3 shows the waveforms of the sequency-ordered Walsh functions with $N = 8$, and the waveforms of sine and cosine functions. As the waveforms of Walsh functions resemble trigonometric functions, it is feasible to replace the trigonometric functions in the Fourier Transform with Walsh functions.

doi:10.6342/NTU202503398

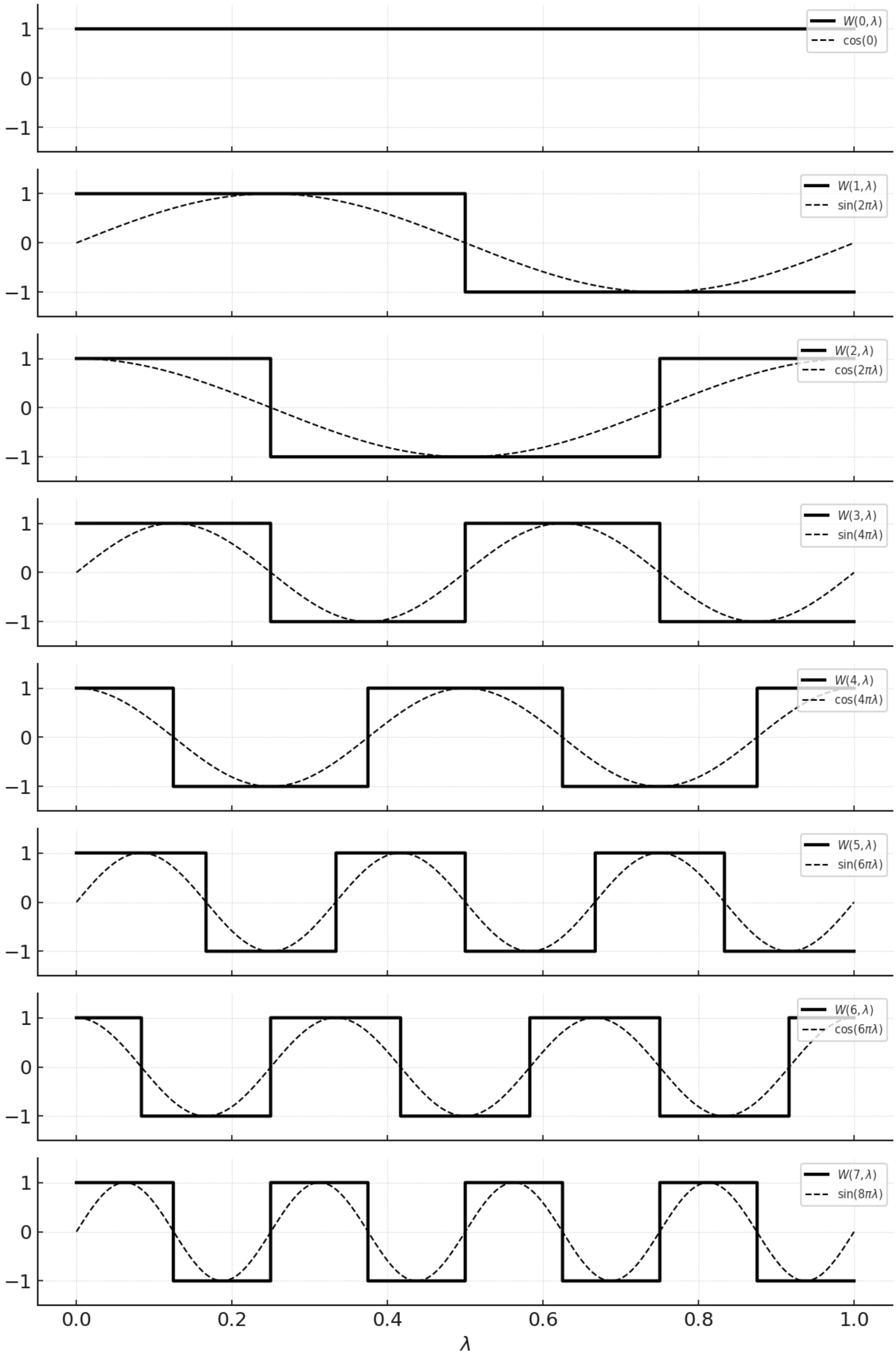

Figure 2.3 Sequency-Ordered Walsh Functions and Trigonometric Comparison

doi:10.6342/NTU202503398

The patterns of the Walsh functions can be generated by the Hadamard matrix H_n.

The base Hadamard matrix H_2 is given by $H_2 = \begin{bmatrix} 1 & 1 \\ 1 & -1 \end{bmatrix}$, and the higher order Hadamard matrix can be generated by the relation $H_{2^n} = \begin{bmatrix} H_{2^{n-1}} & H_{2^{n-1}} \\ H_{2^{n-1}} & -H_{2^{n-1}} \end{bmatrix}$. recursively. In order to gain the sequency-ordered Walsh functions, we need to arrange the rows in sequency ordering.

For example, if $N = 4$, then $H_4 = \begin{bmatrix} H_2 & H_2 \\ H_2 & -H_2 \end{bmatrix} = \begin{bmatrix} 1 & 1 & 1 & 1 \\ 1 & -1 & 1 & -1 \\ 1 & 1 & -1 & -1 \\ 1 & -1 & -1 & 1 \end{bmatrix}$.

After the row arranging in sequency ordering, the sequency-ordered Walsh functions can be gained.

$$H_4' = \begin{bmatrix} 1 & 1 & 1 & 1 \\ 1 & 1 & -1 & -1 \\ 1 & -1 & -1 & 1 \\ 1 & -1 & 1 & -1 \end{bmatrix} = \begin{bmatrix} W(0,\lambda) \\ W(1,\lambda) \\ W(2,\lambda) \\ W(3,\lambda) \end{bmatrix}. \tag{2.11}$$

The sequency of each row of the Hadamard matrix has the relationship below.

Assume the row index is n (started form 0), and the size of the Hadamard matrix is N, then the sequency of each row is:

$$\begin{aligned} &(1)\ \text{For } n < \tfrac{N}{2}, \text{ sequency } = \begin{cases} 2n, & \text{for } n \text{ even} \\ 2n+1, & \text{for } n \text{ odd} \end{cases}. \\ &(2)\ \text{For } n \geq \tfrac{N}{2}, \text{ sequency } = \begin{cases} 2n+1-N, & \text{for } n \text{ even} \\ 2n-N, & \text{for } n \text{ odd} \end{cases}. \end{aligned} \tag{2.12}$$

The Walsh Hadamard transform (WHT) matrix is a normalized Hadamard matrix with its rows arranged in sequency ordering.

For example, if $N = 4$, then the WHT matrix W_4 is given by,

$$W_4 = \frac{1}{\sqrt{4}} \begin{bmatrix} 1 & 1 & 1 & 1 \\ 1 & 1 & -1 & -1 \\ 1 & -1 & -1 & 1 \\ 1 & -1 & 1 & -1 \end{bmatrix} = \frac{1}{\sqrt{4}} \begin{bmatrix} W(0,\lambda) \\ W(1,\lambda) \\ W(2,\lambda) \\ W(3,\lambda) \end{bmatrix} = W_4^T. \tag{2.13}$$

doi:10.6342/NTU202503398

The WHT can be regarded as a special case within the broader class of discrete Fourier transforms (DFTs).

The OTSM modulation process mirrors the structure of OTFS but substitutes the IFFT and FFT matrix with the WHT matrix.

In matrix form, at the transmitter, $S = G_{tx}X_{DD}W_N$, and at the receiver, $Y_{DD} = G_{rx}RW_N$.

2.4 Channel Model

The input-output relation in OTFS/OTSM system can be written as

$$r(t) = \int\int h_{DD}(\tau,\nu)s(t-\tau)e^{j2\pi\nu(t-\tau)}d\tau d\nu + w(t). \tag{2.14}$$

, where $h_{DD}(\tau,\nu)$ is the DD domain channel matrix, and $w(t)$ is Additive White Gaussian Noise (AWGN) [1], [2], [7].

The DD domain channel matrix $h_{DD}(\tau,\nu)$ can be modeled as

$$h_{DD}(\tau,\nu) = \sum_{i=1}^{P} h_i\delta(\tau-\tau_i)\delta(\nu-\nu_i). \tag{2.15}$$

, where P is the number of propagation paths, h_i, τ_i, ν_i denote the complex path gain, delay, and Doppler shift (or frequency) associated with the i-th path.

In order to express the delay and the Doppler shift on the DD domain, we need to convert these numbers into taps. The delay taps are $l_i = \tau_i M\Delta f$, and the Doppler taps are $k_i = \nu_i NT$, where l_i are assumed to be integers.

This sparse representation means most entries in the DD grid are zero, with only a few taps significantly contributing to the overall channel response.

In matrix form, $r = G \cdot s + w$, where G is the time domain channel matrix, and w is AWGN.

doi:10.6342/NTU202503398

The time domain channel matrix can be expressed as

$$G = \sum_{i=1}^{P} h_i \Pi^{l_i} \Delta^{k_i} \in \mathbb{C}^{MN \times MN}. \tag{2.16}$$

, where $\Pi = \begin{bmatrix} 0 & \cdots & 0 & 1 \\ 1 & \ddots & 0 & 0 \\ \vdots & \ddots & \vdots & \vdots \\ 0 & \cdots & 1 & 0 \end{bmatrix} \in \mathbb{C}^{MN \times MN}$ is the permutation matrix which cyclically shifts the signal, and $\Delta = diag(z^0, z^1, \dots, z^{MN-1}), \in \mathbb{C}^{MN \times MN}$ is a diagonal matrix with $z = e^{\frac{j2\pi}{MN}}$.

Once the time domain channel matrix G is obtained, Minimum Mean Square Error (MMSE) detection can be applied for channel equalization, as expressed by:

$$\hat{s} = (G^H \cdot G + \sigma^2 I_{MN})^{-1} G^H r. \tag{2.17}$$

There are many research channel equalization methods for OTFS and OTSM system [5], [12], [13], [14], [15], [16]; however, we only use MMSE detection in the thesis.

2.5 Blockwise MMSE Implementation

In conventional OTFS and OTSM systems, the entire transmit frame is processed as a monolithic block. However, processing the entire frame as a single block can be computationally inefficient. To address this issue, blockwise implementation divides the signal, channel, and detection process into manageable sub-blocks, significantly reducing complexity while retaining performance advantages [4], [10].

We use the matrix form input-output relation mentioned above, $r = G \cdot s + w$.

To reduce complexity, instead of processing the entire signal vector at once, we divide it into N blocks, each size of M, corresponding to one time slot (or sequency index).

We define $s_n \in \mathbb{C}^{M \times 1}, r_n \in \mathbb{C}^{M \times 1}, G_n \in \mathbb{C}^{M \times M}$, then we will get the relation:

doi:10.6342/NTU202503398

$$r_n[m] = \sum_{l, l \le m} G_n[l,m] s_n[m-l] + \sum_{l, l > m} G_n[l,m] s_{n-1}[[m-l]_M] + w_n. \quad (2.18)$$

, where $l \in \mathcal{L} = \{0, \dots, l_{max}\}$ be the delay taps and l_{max} denote the largest delay tap. We can find that there is an ISI term from s_{n-1}, in order to solve this problem, we need to add zeros to the last rows of the complex information symbols on DD domain $X_{DD}[l,k]$ with at least length l_{max}. This zero-padding ensures that ISI from preceding blocks is eliminated, allowing each block to be detected independently.

The blockwise input-output relation can be written as

$$r_n = G_n \cdot s_n + w_n. \quad (2.19)$$

, and the blockwise MMSE detection can be implemented by the equation

$$\hat{s}_n = (G_n^H \cdot G_n + \sigma^2 I_M)^{-1} G_n^H r_n. \quad (2.20)$$

2.6 Interpolation Pilot-Based Channel Estimation Method

Accurate channel estimation is essential for reliable symbol detection in OTFS and OTSM systems, especially under rapidly time-varying and frequency-selective channels. To address this, many channel estimation methods have been proposed [5], [9], [11], [12], [13].

In this section, we introduce a pilot-based time domain interpolation channel estimation method [4].

Recall that zero padding is added to the last rows of OTFS/OTSM symbols; this space can be utilized for pilot insertion. The pilot also requires additional zero padding of at least length l_{max} as a guard interval to prevent interference from adjacent data symbols.

We can write down the symbols in the DD domain data grid below.

doi:10.6342/NTU202503398

$$x_m(n) = \begin{cases} x_p\delta[n-n_p] & , if\ m = m_p \\ 0 & , if\ 0 < |m-m_p| \leq l_{max} \\ data & , otherwise \end{cases} . \quad (2.21)$$

Here, we place the pilot x_p at (m_p, n_p) with the pilot power E_p.

The pilot power E_p is selected by the relation $E_p = \beta N l_{max} E_s$, where β is a weighting factor, and E_s is the average energy of the DD domain information symbols.

After the N-point FFT/WHT, the pilot will separate to N time slots, the equations are given below.

In OTFS (IFFT):

$$\tilde{x}_{mp} = F_N^H \cdot x_{m_p} = [F_N^H(n_p, 0), \dots, F_N^H(n_p, N-1)]. \quad (2.22)$$

In OTSM (WHT):

$$\tilde{x}_{m_p} = W_N \cdot x_{m_p} = x_p[W_N(n_p, 0), \dots, W_N(n_p, N-1)]. \quad (2.23)$$

The input-output relation of the pilots can be express as:

$$\tilde{y}_{(m_p+1)}(n) = \sum_{l' \in \mathcal{L}} G(l', m_p + l + nM)\tilde{x}_{(m_p+l-l')}(n) + w(n). \quad (2.24)$$

The estimated channel coefficients $G(l', m_p + l + nM)$ can be easily estimated by dividing the received pilots by the transmitted pilots.

$$G(l', m_p + l + nM) = \frac{\tilde{y}_{(m_p+1)}(n)}{\tilde{x}_{m_p}(n)}. \quad (2.25)$$

Noting here the AWGN term $w(n)$ is ignored because of the high pilot power.

This operation provides channel information for each delay across all time slots, enabling interpolation to estimate the channel response across discrete time slots.

There are two methods to reconstruct the channel curve. The first method is linear interpolation, and the second method is cubic spline interpolation [18]. The cubic spline interpolation will have more accurate performance at the cost of computational complexity.

doi:10.6342/NTU202503398

2.7 Summary

In this chapter, we reviewed the essentials of OFDM, OTFS, and OTSM modulation schemes for combating multipath fading and Doppler effects.

We saw how OFDM's cyclic-prefix approach preserves subcarrier orthogonality under static channels but struggles in high-mobility scenarios. OTFS was introduced as a 2-D modulation in the delay–Doppler domain, exploiting channel sparsity to improve robustness under time-varying conditions, while OTSM replaces Fourier transforms with Walsh–Hadamard transforms to achieve similar resilience at lower computational cost.

We then developed a unified channel model in the DD domain, leading to blockwise MMSE detection that reduces complexity by processing the frame in subblocks.

Finally, we detailed a pilot-based interpolation channel estimator—placing pilots in zero-padded guard intervals and reconstructing the channel over time slots via linear or spline interpolation—to obtain accurate channel estimates with manageable overhead.

doi:10.6342/NTU202503398

第三章　Channel Estimation Methods for MIMO System

In the previous chapter, we focused on single-input single-output (SISO) systems, where the transmitter and receiver are each equipped with a single antenna. While SISO models provide valuable insights into modulation schemes such as OFDM, OTFS, and OTSM under various channel conditions, they are inherently limited in terms of capacity and diversity gains.

Modern wireless communication systems increasingly adopt multiple-input multiple-output (MIMO) configurations, where both the transmitter and receiver employ multiple antennas. MIMO technology enables significant enhancements in spectral efficiency, link reliability, and system throughput by exploiting spatial multiplexing and diversity gains.

However, these benefits come with added complexity — particularly in the domain of channel estimation. Unlike in SISO systems, where the channel can be modeled as a single scalar or vector, MIMO channels are characterized by matrix-valued responses, capturing the interactions between each transmit-receive antenna pair. This introduces new challenges in accurate channel modeling, estimation, and equalization, especially in time-varying and frequency-selective environments.

In this chapter, we extend the analysis of channel estimation techniques from SISO to MIMO systems. We explore pilot-based channel estimation methods designed to address the increased dimensionality of MIMO channels, discuss blockwise detection strategies suitable for multi-antenna configurations, and investigate the performance of these methods under various practical scenarios.

doi:10.6342/NTU202503398

3.1 MIMO OTFS/OTSM System Structure

A typical system structure of 2×2 MIMO OTFS/OTSM system is shown in Figure 3.1.

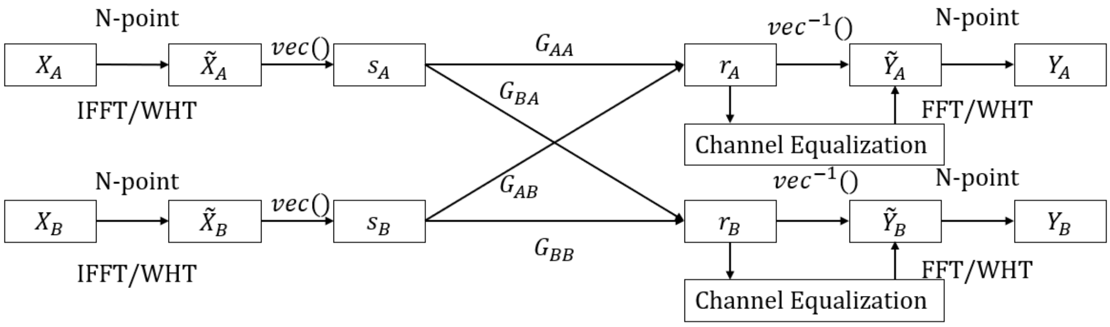

Figure 3.1 2×2 MIMO OTFS/OTSM System Model

In the 2×2 MIMO system, we denote $s = \begin{bmatrix} s_A \\ s_B \end{bmatrix} \in \mathbb{C}^{2MN\times 1}$ be the transmitted signal, $r = \begin{bmatrix} r_A \\ r_B \end{bmatrix} \in \mathbb{C}^{2MN\times 1}$ be the received signal, and $G = \begin{bmatrix} G_{AA} & G_{AB} \\ G_{BA} & G_{BB} \end{bmatrix} \in \mathbb{C}^{2MN\times 2MN}$ be the channel matrix.

The input-output relation in matrix form can be expressed as

$$r = G \cdot s + w. \tag{3.1}$$

, where $w = \begin{bmatrix} w_A \\ w_B \end{bmatrix} \in \mathbb{C}^{2MN\times 1}$ be AWGN.

The matrix form resembles that of a SISO system, allowing the use of MMSE detection to estimate the transmitted signal.

$$\hat{s} = (G^H \cdot G + \sigma^2 I_{2MN})^{-1} G^H r. \tag{3.2}$$

Furthermore, blockwise MMSE detection can be applied to the 2×2 MIMO system.

We can divide $s_A, s_B, r_A, r_B, G_{AA}, G_{AB}, G_{BA}, G_{BB}$ into N blocks.

Assume $s_A = \begin{bmatrix} s_{A0} \\ s_{A1} \\ \vdots \\ s_{A(N-1)} \end{bmatrix}, s_B = \begin{bmatrix} s_{B0} \\ s_{B1} \\ \vdots \\ s_{B(N-1)} \end{bmatrix}$, then $s = \begin{bmatrix} s_0 \\ s_1 \\ \vdots \\ s_{(N-1)} \end{bmatrix}$, where $s_n = \begin{bmatrix} s_{An} \\ s_{Bn} \end{bmatrix} \in$

doi:10.6342/NTU202503398

$\mathbb{C}^{2M\times 1}$; similarly, $r_A = \begin{bmatrix} r_{A0} \\ r_{A1} \\ \vdots \\ r_{A(N-1)} \end{bmatrix}, r_B = \begin{bmatrix} r_{B0} \\ r_{B1} \\ \vdots \\ r_{B(N-1)} \end{bmatrix}$, then $r = \begin{bmatrix} r_0 \\ r_1 \\ \vdots \\ r_{(N-1)} \end{bmatrix}$, where $r_n = \begin{bmatrix} r_{An} \\ r_{Bn} \end{bmatrix} \in \mathbb{C}^{2M\times 1}$.

For the channel matrix,

$$G_{AA} = \begin{bmatrix} G_{AA0} & 0 & 0 & 0 \\ 0 & G_{AA1} & 0 & 0 \\ 0 & 0 & \ddots & 0 \\ 0 & 0 & 0 & G_{AA(N-1)} \end{bmatrix}, G_{AB} = \begin{bmatrix} G_{AB0} & 0 & 0 & 0 \\ 0 & G_{AB1} & 0 & 0 \\ 0 & 0 & \ddots & 0 \\ 0 & 0 & 0 & G_{AB(N-1)} \end{bmatrix},$$

$$G_{BA} = \begin{bmatrix} G_{BA0} & 0 & 0 & 0 \\ 0 & G_{BA1} & 0 & 0 \\ 0 & 0 & \ddots & 0 \\ 0 & 0 & 0 & G_{BA(N-1)} \end{bmatrix}, G_{BB} = \begin{bmatrix} G_{BB0} & 0 & 0 & 0 \\ 0 & G_{BB1} & 0 & 0 \\ 0 & 0 & \ddots & 0 \\ 0 & 0 & 0 & G_{BB(N-1)} \end{bmatrix}$$

, then $G = \begin{bmatrix} G_0 & 0 & 0 & 0 \\ 0 & G_1 & 0 & 0 \\ 0 & 0 & \ddots & 0 \\ 0 & 0 & 0 & G_{(N-1)} \end{bmatrix}$, where $G_n = \begin{bmatrix} G_{AAn} & G_{ABn} \\ G_{BAn} & G_{BBn} \end{bmatrix} \mathbb{C}^{2M\times 2M}$.

Now, we can write down the blockwise input-output relation:

$$r_n = G_n \cdot s_n + w_n. \tag{3.3}$$

The blockwise MMSE detection equation is identical to that of the SISO system.

$$\hat{s}_n = (G_n^H \cdot G_n + \sigma^2 I_M)^{-1} G_n^H r_n. \tag{3.4}$$

3.2 Multiple Pilots Channel Estimation Method

In 2×2 MIMO system, we want to use the interpolation pilot-based channel estimation method mentioned above in SISO case. However, we have four different independent channel matrices instead of one channel matrix. Without modification, at receiver A, the channel components G_{AA} and G_{AB} with the same delay index would interfere with each other, rendering the channel estimation ineffective.

One introduces an adjustment to solve this problem, using multiple pilots [5]. For

doi:10.6342/NTU202503398

an 2×2 MIMO system, we place two different pilots on different subcarrier index n, along with their own guard symbols.

For example, at transmitter A, we only use pilot A and leave pilot B be zero; while at transmitter B, we only use pilot B and leave pilot A be zero too.
The advantage of this method is that separating pilots in the DD domain prevents interference between channel components at the receivers.

However, allocating separate zero-padding regions for each pilot introduces significant overhead, especially as the number of MIMO antennas increases.

3.3 Proposed Channel Estimation Method

In order to solve the huge overhead problem, we introduce an 2×2 MIMO channel estimation method with one pilot as the same as the channel estimation method what we mentioned above in SISO system. However, since the channel components at one receiver can still interfere with each other, we propose a method to separate these mixed signals.

3.3.1 First-ordered Channel Estimation

At one receiver, we assume the channel information in every four continuous time slots are linear, for example, at receiver A, for time slot index 0,1,2,3 at delay 0. The channel coefficients from G_{AA} are $g_{aa0}, g_{aa1}, g_{aa2}, g_{aa3}$, and the channel coefficients from G_{AB} are $g_{ab0}, g_{ab1}, g_{ab2}, g_{ab3}$. Assuming $g_{aa0}, g_{aa1}, g_{aa2}, g_{aa3}$ are linear and $g_{ab0}, g_{ab1}, g_{ab2}, g_{ab3}$ are linear. We can write down the equations:

doi:10.6342/NTU202503398

$$g_{aax} = x \cdot aa_1 + aa_0,$$

$$g_{abx} = x \cdot ab_1 + ab_0 \tag{3.5}$$

$$\text{for } x \in \{0,1,2,3\}.$$

The corresponding received pilot signals are $r_{pa0}, r_{pa1}, r_{pa2}, r_{pa3}$, where $r_{pax} = g_{aax} + g_{abx}$ for $x \in \{0,1,2,3\}$.

We can write these relations into a matrix:

$$\begin{bmatrix} r_{pa0} \\ r_{pa1} \\ r_{pa2} \\ r_{pa3} \end{bmatrix} = \begin{bmatrix} 1 & 1 & 0 & 0 \\ 1 & 1 & 1 & 1 \\ 1 & 1 & 2 & 2 \\ 1 & 1 & 3 & 3 \end{bmatrix} \begin{bmatrix} aa_0 \\ ab_0 \\ aa_1 \\ ab_1 \end{bmatrix} \Rightarrow \overrightarrow{r_{pa}} = A\overrightarrow{g_a}. \tag{3.6}$$

With the matrix form, we can try to get the channel coefficients $\overrightarrow{g_a}$ from $\overrightarrow{r_{pa}}$ using Least Square (LS) method. The equation is given by:

$$\overrightarrow{g_a} = (A^H A)^{-1} A^H \overrightarrow{r_{pa}}. \tag{3.7}$$

However, since matrix A is singular, the LS method cannot be directly applied. To address this issue, we introduce a sign alternation scheme for pilot transmission. To make matrix A full rank, we apply an alternating sign scheme to the pilot symbols: $+1, +1, -1, -1$ for transmitter A, $+1, -1, +1, -1$ for transmitter B.

This adjustment results in the modified received pilot equation matrix:

$$\begin{bmatrix} r_{pa1} \\ r_{pa2} \\ r_{pa3} \\ r_{pa4} \end{bmatrix} = \begin{bmatrix} 1 & 1 & 0 & 0 \\ 1 & -1 & 1 & -1 \\ -1 & 1 & -2 & 2 \\ -1 & -1 & -3 & -3 \end{bmatrix} \begin{bmatrix} aa_0 \\ ab_0 \\ aa_1 \\ ab_1 \end{bmatrix} \Rightarrow \overrightarrow{r_{pa}} = A\overrightarrow{g_a}. \tag{3.8}$$

With this transformation, matrix A becomes invertible, allowing us to use LS method to get the channel coefficients.

3.3.2 Second-ordered Channel Estimation

Since the first-ordered channel estimation can work properly, we should try higher ordered channel estimation methods to increase the accuracy.

doi:10.6342/NTU202503398

At one receiver, we assume the channel information in every six continuous time slots are on a second-ordered curve, for example, at receiver A, for time slot index 0,1,2,3,4,5 at delay 0. The channel coefficients from G_{AA} are $g_{aa0}, g_{aa1}, g_{aa2}, g_{aa3}, g_{aa4}, g_{aa5}$, and the channel coefficients from G_{AB} are $g_{ab0}, g_{ab1}, g_{ab2}, g_{ab3}, g_{ab4}, g_{ab5}$. Assuming the six points $g_{aa0}, g_{aa1}, g_{aa2}, g_{aa3}, g_{aa4}, g_{aa5}$ are on a second-ordered curve and the six points $g_{ab0}, g_{ab1}, g_{ab2}, g_{ab3}, g_{ab4}, g_{ab5}$ are on a second-ordered curve. We can write down the equations:

$$\begin{gathered} g_{aax} = x^2 \cdot aa_2 + x \cdot aa_1 + aa_0, \\ g_{abx} = x^2 \cdot ab_2 + x \cdot ab_1 + ab_0, \\ \text{for } x \in \{0,1,2,3,4,5\}. \end{gathered} \tag{3.9}$$

We can write these relations into a matrix:

$$\begin{bmatrix} r_{pa0} \\ r_{pa1} \\ r_{pa2} \\ r_{pa3} \\ r_{pa4} \\ r_{pa5} \end{bmatrix} = \begin{bmatrix} 1 & 1 & 0 & 0 & 0 & 0 \\ 1 & 1 & 1 & 1 & 1 & 1 \\ 1 & 1 & 2 & 2 & 4 & 4 \\ 1 & 1 & 3 & 3 & 9 & 9 \\ 1 & 1 & 4 & 4 & 16 & 16 \\ 1 & 1 & 5 & 5 & 25 & 25 \end{bmatrix} \begin{bmatrix} aa_0 \\ ab_0 \\ aa_1 \\ ab_1 \\ aa_2 \\ ab_2 \end{bmatrix} \Rightarrow \overrightarrow{r_{pa}} = A\overrightarrow{g_a}. \tag{3.10}$$

Similarly, since matrix A is singular, the LS method cannot be applied directly.

To make matrix A full rank, we apply an alternating sign scheme to the pilot symbols: $+1, +1, -1, -1, +1, +1$ for transmitter A, $+1, -1, +1, -1, +1, -1$ for transmitter B.,

This adjustment results in the modified received pilot equation matrix:

$$\begin{bmatrix} r_{pa0} \\ r_{pa1} \\ r_{pa2} \\ r_{pa3} \\ r_{pa4} \\ r_{pa5} \end{bmatrix} = \begin{bmatrix} 1 & 1 & 0 & 0 & 0 & 0 \\ 1 & -1 & 1 & -1 & 1 & -1 \\ -1 & 1 & -2 & 2 & -4 & 4 \\ -1 & -1 & -3 & -3 & -9 & -9 \\ 1 & 1 & 4 & 4 & 16 & 16 \\ 1 & -1 & 5 & -5 & 25 & -25 \end{bmatrix} \begin{bmatrix} aa_0 \\ ab_0 \\ aa_1 \\ ab_1 \\ aa_2 \\ ab_2 \end{bmatrix} \Rightarrow \overrightarrow{r_{pa}} = A\overrightarrow{g_a}. \tag{3.11}$$

doi:10.6342/NTU202503398

With this transformation, matrix A becomes invertible, allowing us to use LS method to get the channel coefficients.

3.3.3 Third-ordered Channel Estimation

The third-ordered channel estimation can also be implemented from the process above. At one receiver, we assume the channel information in every eight continuous time slots are on a third-ordered curve, for example, at receiver A, for time slot index 0,1,2,3,4,5,6,7 at delay 0. The channel coefficients from G_{AA} are $g_{aa0}, g_{aa1}, g_{aa2}, g_{aa3}, g_{aa4}, g_{aa5}, g_{aa6}, g_{aa7}$, and the channel coefficients from G_{AB} are $g_{ab0}, g_{ab1}, g_{ab2}, g_{ab3}, g_{ab4}, g_{ab5}, g_{ab6}, g_{ab7}$. Assuming the eight points $g_{aa0}, g_{aa1}, g_{aa2}, g_{aa3}, g_{aa4}, g_{aa5}, g_{aa6}, g_{aa7}$ are on a third-ordered curve and the six points $g_{ab0}, g_{ab1}, g_{ab2}, g_{ab3}, g_{ab4}, g_{ab5}, g_{ab6}, g_{ab7}$ are on a third-ordered curve. We can write down the equations:

$$\begin{gathered} g_{aax} = x^3 \cdot aa_3 + x^2 \cdot aa_2 + x \cdot aa_1 + aa_0, \\ g_{abx} = x^3 \cdot ab_3 + x^2 \cdot ab_2 + x \cdot ab_1 + ab_0, \\ \text{for } x \in \{0,1,2,3,4,5,6,7\}. \end{gathered} \tag{3.12}$$

We can write these relations into a matrix:

$$\begin{bmatrix} r_{pa0} \\ r_{pa1} \\ r_{pa2} \\ r_{pa3} \\ r_{pa4} \\ r_{pa5} \\ r_{pa6} \\ r_{pa7} \end{bmatrix} = \begin{bmatrix} 1 & 1 & 0 & 0 & 0 & 0 & 0 & 0 \\ 1 & 1 & 1 & 1 & 1 & 1 & 1 & 1 \\ 1 & 1 & 2 & 2 & 4 & 4 & 8 & 8 \\ 1 & 1 & 3 & 3 & 9 & 9 & 27 & 27 \\ 1 & 1 & 4 & 4 & 16 & 16 & 64 & 64 \\ 1 & 1 & 5 & 5 & 25 & 25 & 125 & 125 \\ 1 & 1 & 6 & 6 & 36 & 36 & 216 & 216 \\ 1 & 1 & 7 & 7 & 49 & 49 & 343 & 343 \end{bmatrix} \begin{bmatrix} aa_0 \\ ab_0 \\ aa_1 \\ ab_1 \\ aa_2 \\ ab_2 \\ aa_3 \\ ab_3 \end{bmatrix} \Rightarrow \overrightarrow{r_{pa}} = A\overrightarrow{g_a}. \tag{3.13}$$

Similarly, the matrix A is not invertible, we cannot apply the LS method to get channel coefficient $\overrightarrow{g_a}$.

doi:10.6342/NTU202503398

To make matrix A full rank, we apply an alternating sign scheme to the pilot symbols: $+1, +1, -1, -1, +1, +1, -1, -1$ for transmitter A, $+1, -1, +1, -1, +1, -1, +1, -1$ for transmitter B.,

This adjustment results in the modified received pilot equation matrix:

$$\begin{bmatrix} r_{pa0} \\ r_{pa1} \\ r_{pa2} \\ r_{pa3} \\ r_{pa4} \\ r_{pa5} \\ r_{pa6} \\ r_{pa7} \end{bmatrix} = \begin{bmatrix} 1 & 1 & 0 & 0 & 0 & 0 & 0 & 0 \\ 1 & -1 & 1 & -1 & 1 & -1 & 1 & -1 \\ -1 & 1 & -2 & 2 & -4 & 4 & -8 & 8 \\ -1 & -1 & -3 & -3 & -9 & -9 & -27 & -27 \\ 1 & 1 & 4 & 4 & 16 & 16 & 64 & 64 \\ 1 & -1 & 5 & -5 & 25 & -25 & 125 & -125 \\ -1 & 1 & -6 & 6 & -36 & 36 & -216 & 216 \\ -1 & -1 & -7 & -7 & -49 & -49 & -343 & -343 \end{bmatrix} \begin{bmatrix} aa_0 \\ ab_0 \\ aa_1 \\ ab_1 \\ aa_2 \\ ab_2 \\ aa_3 \\ ab_3 \end{bmatrix} \tag{3.14}$$

$$\Rightarrow \overrightarrow{r_{pa}} = A\overrightarrow{g_a}.$$

With this transformation, matrix A becomes invertible, allowing us to use LS method to get the channel coefficients.

3.3.4 Modifications and Improvements

The proposed channel estimation method works nearly similar to the multiple pilots channel estimation method at low speed (e.g., 120 km/hr); however, we suffer severe overshoot when at high speed (e.g., 500 km/hr or higher). This issue arises because only a limited number of points are used to reconstruct the curve (e.g., six points for second-order estimation). Therefore, several improvements are proposed.

1. Select the middle of reconstructed curves.

   Since we severe serious overshoot from the reconstructed curves, we can choose the middle curve of the reconstructed curves to avoid the overshoot area on the edge. On the contrary, we need to reconstruct more curves and build more LS method matrices A, which increase the computational complexity. This modification indeed improves the Normalized Mean Square Error (NMSE) between the estimated and actual channels.

doi:10.6342/NTU202503398

2. Compute a weighted average of all reconstructed curves.

   This modification is a small revised version of the modification mentioned above. We need to reconstruct more curves and build more LS method matrices A as the modification above. The difference is, we do not discard the edge of the reconstructed curves, but adding all the reconstructed curves together and divide them by how many times the channel coefficient of one time index has been added. This adjustment also enhances the NMSE performance between the estimated and actual channels. This method can also be called "moving average" method.

3. Reconstruct a new curve using all sample points.

   If we have a look back to the SISO interpolation pilot-based channel estimation method which we mentioned at Chapter 2.6, we will find out the method use all the sample points to reconstruct a new curve. When applied to the MIMO case, this implementation significantly reduces overshoot in the reconstructed curves by using a single curve fitted to many sample points. Among the three proposed modifications, it yields the best NMSE performance.

After these modifications implementing in the proposed method, we can nearly have the same NMSE performance compared with the multiple pilots channel estimation method which we mentioned above at low speed (e.g., 250 km/hr and below); while at higher speeds (e.g., 500 km/h), the NMSE performance with the modifications is significantly better than without them.

3.4 Summary

Building on the SISO framework, this chapter extended channel estimation and equalization to 2×2 MIMO configurations. We first reviewed blockwise MMSE detection for the full MIMO channel matrix, then explored a multi-pilot scheme that

doi:10.6342/NTU202503398

assigns distinct pilots per transmit antenna to avoid mutual interference at the receiver.

To reduce the significant pilot overhead of that approach, we proposed a novel single-pilot method using sign-alternating patterns and polynomial fitting. First-, second-, and third-order curve fits were derived to extract both self- and cross-antenna channel coefficients via least-squares, with each requiring a tailored sign pattern to ensure invertibility.

We also introduced three enhancements—a middle-curve selection, moving-average fusion of reconstructed curves, and full-frame curve fitting—that substantially improve estimation accuracy, especially in high-Doppler scenarios.

doi:10.6342/NTU202503398

第四章　Numerical Results

This chapter presents simulation results that validate the theoretical models and algorithms discussed earlier. Focusing on BER performance and channel estimation accuracy under various mobility scenarios, we assess both SISO and MIMO systems using blockwise MMSE and pilot-based estimation methods. These results demonstrate the practical effectiveness and limitations of the proposed techniques in realistic channel conditions.

The channel model used in all the simulations below is Extended Vehicular A Model (EVA), ruled by 3GPP [17]. The channel model has nine channel taps, and the channel delay and relative power of each tap are distinct, shown in Table 4.1 below.

Excess tap delay [ns]	Relative power [dB]
0	0.0
30	-1.5
150	-1.4
310	-3.6
370	-0.6
710	-9.1
1090	-7.0
1730	-12.0
2510	-16.9

Table 4.1 Channel Delay Profile and Relative Power of 3GPP EVA Model [17]

As for the Doppler frequency for each tap, it is determined by Jake's Formula:

$$\nu_i = \nu_{max} cos\theta_i, \theta_i \in [-\pi, \pi], \text{ for } i \in \{0,1,\dots,8\}. \tag{4.1}$$

, where the term ν_{max} is the max speed of the channel. The simulations choose 0 km/hr, 30 km/hr, 120 km/hr, 250 km/hr, 500 km/hr, and 1000 km/hr to simulation the BER performance under different speeds.

doi:10.6342/NTU202503398

4.1 SISO System

In SISO system, we focus on the Bit Error Rate (BER) performance of OTFS and OTSM system, alongside with blockwise MMSE Equalization implementation on both system. We then examine the NMSE performance of the interpolation pilot-based channel estimation method.

4.1.1 OTFS and OTSM System

The parameters of the simulation are shown in the Table 4.2 below

Parameters	**Value**
M	64
N	64
Modulation	4-QAM
Carrier frequency	4Ghz
Subcarrier spacing	15khz
Channel	EVA
Channel Estimation	Perfect CSI
Channel Equalization	MMSE

Table 4.2 Simulation Parameters for OTFS/OTSM System Performance Evaluation

The BER performances of OTFS and OTSM are shown in Figures 4.1 and 4.2.

doi:10.6342/NTU202503398

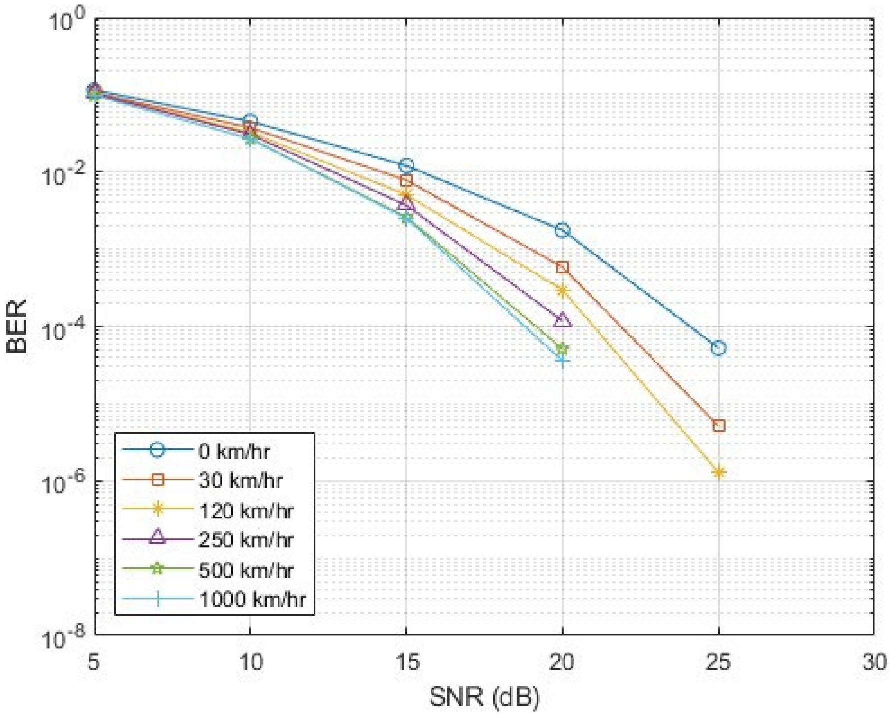

Figure 4.1 BER Performance of OTFS under EVA Channel

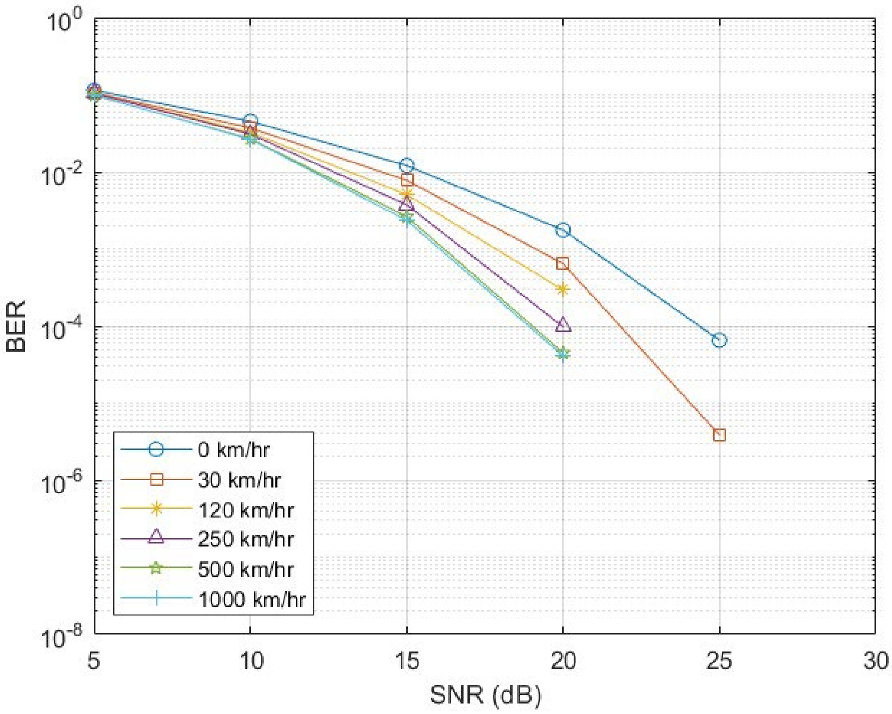

Figure 4.2 BER Performance of OTSM under EVA Channel

The simulation results indicate that OTFS and OTSM exhibit nearly identical BER performance under the given parameters.

doi:10.6342/NTU202503398

4.1.2 Blockwise MMSE Equalization

In this simulation, we divide the transmitted signal, received signal and the channel matrix into N blocks and use the same parameters as same as the previous chapter. The BER performances of OTFS with conventional MMSE equalization and with blockwise MMSE equalization are shown in Figures 4.3 and 4.4.

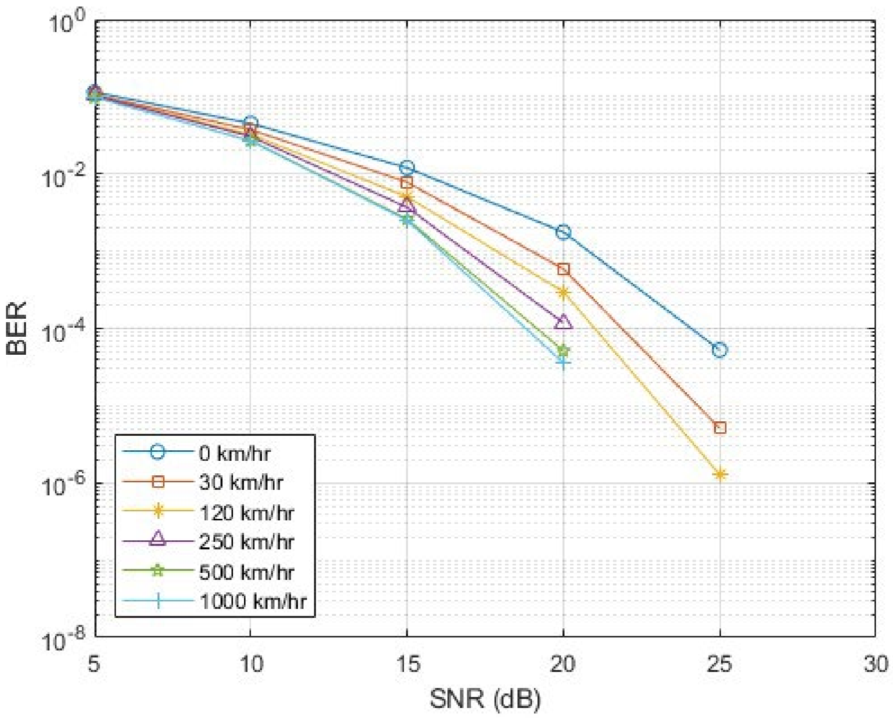

Figure 4.3 BER of OTFS with Conventional MMSE Equalization

doi:10.6342/NTU202503398

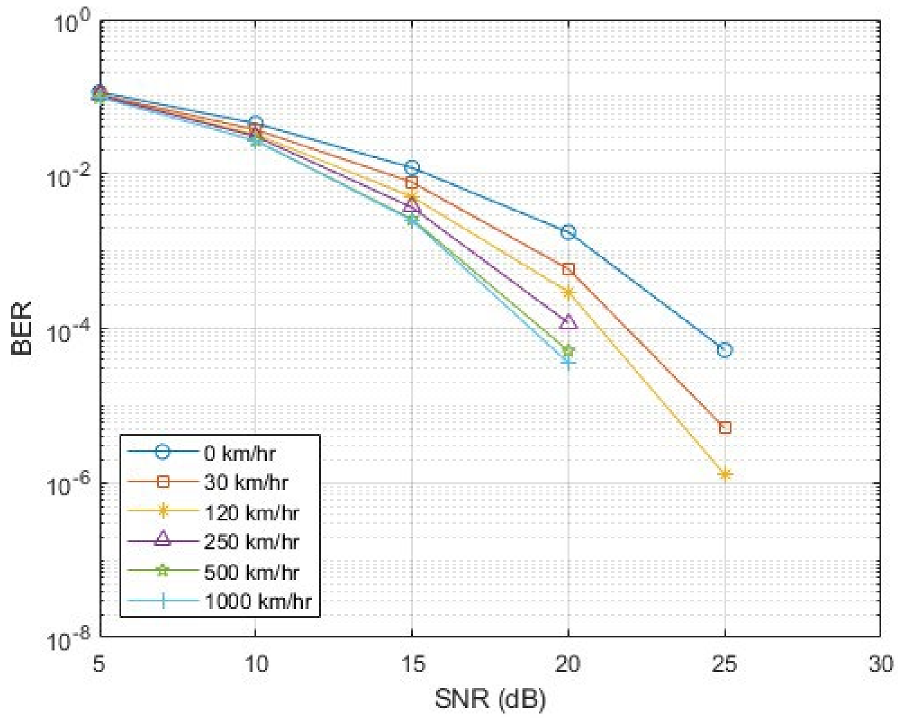

Figure 4.4 BER of OTFS with Blockwise MMSE Equalization

The BER performance OTSM with MMSE equalization and with blockwise MMSE equalization are shown in the Figure 4.5 and Figure 4.6 below.

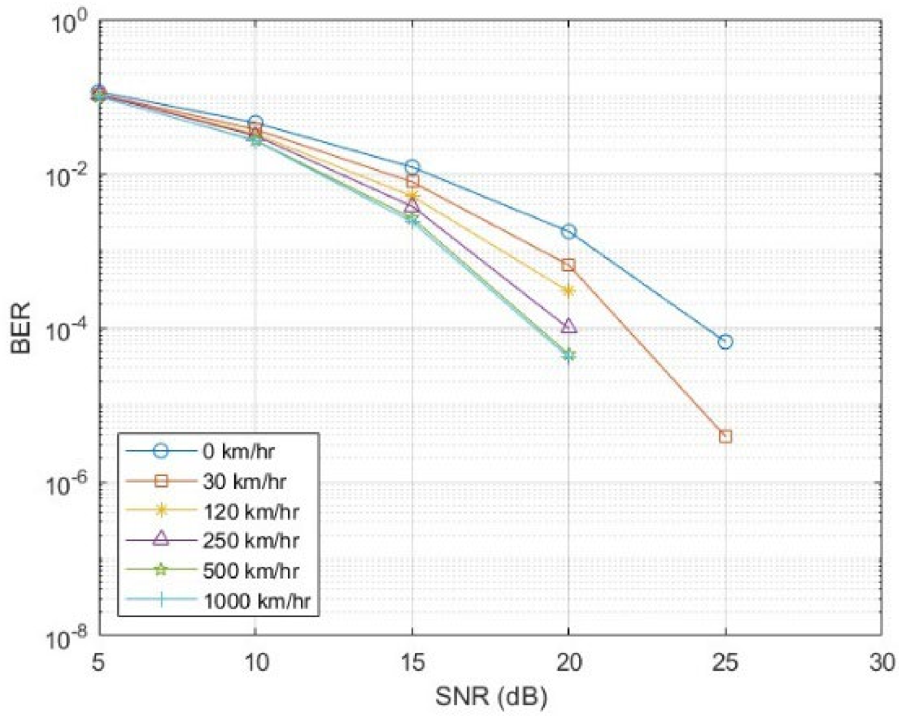

Figure 4.5 BER of OTSM with Conventional MMSE Equalization

doi:10.6342/NTU202503398

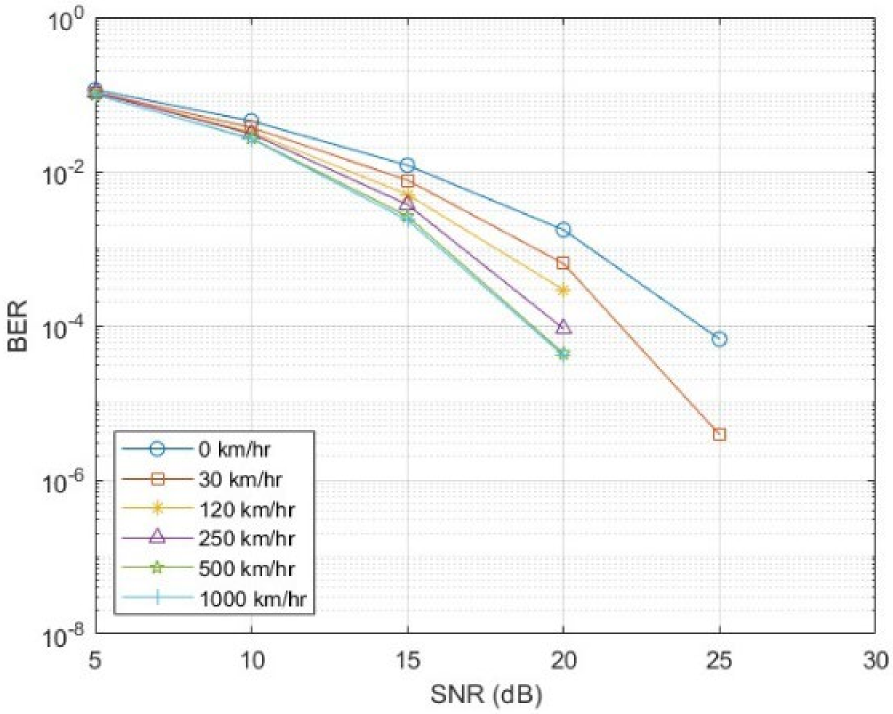

Figure 4.6 BER of OTSM with Blockwise MMSE Equalization

From the simulation results above, we can see that OTFS and OTSM system have nearly the same BER performance with or without blockwise implementation under these parameters, indicating that blockwise MMSE equalization can be used in subsequent simulations with negligible BER degradation and improved computational efficiency.

4.1.3 Interpolation Pilot-based Channel Estimation Method

In this simulation, we place the pilot on delay index 61 and Doppler index 0 on the DD grid with the guard symbol length 3 rows, the other parameters are the same as the previous chapters. The BER performance at high speed (500 km/hr and 1000 km/hr) is shown in Figure 4.7.

doi:10.6342/NTU202503398

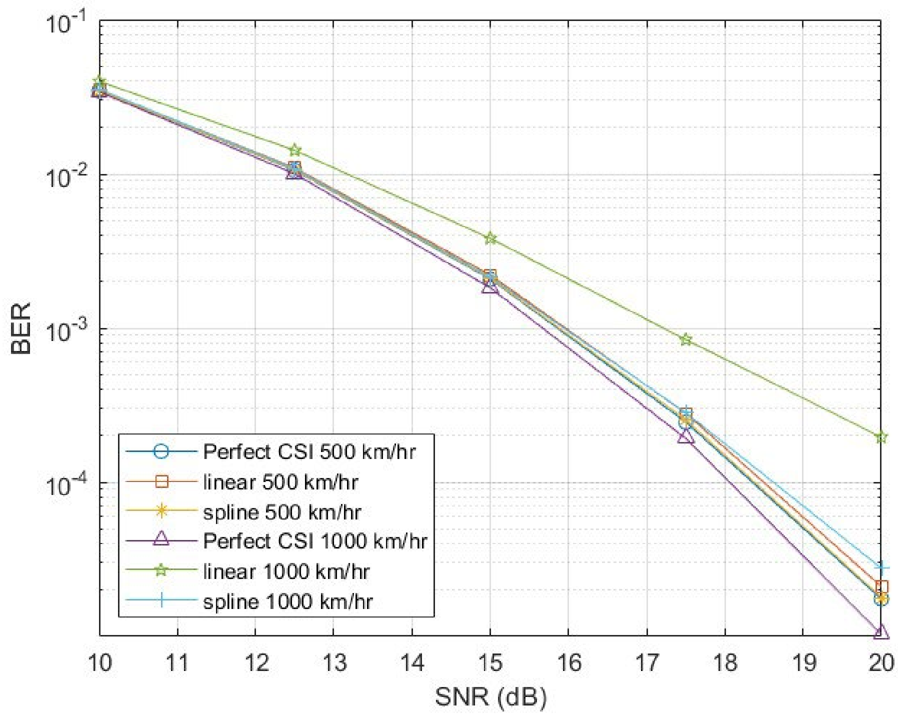

Figure 4.7 BER of OTFS/OTSM with Interpolation Pilot-Based Channel Estimation

In this simulation, two interpolation methods are employed: first-order linear interpolation and third-order spline interpolation. The results show that third-order spline interpolation closely matches the BER performance achieved with perfect CSI, even at 1000 km/hr.

4.2 MIMO System

In the previous chapter, we perform the BER performance of OTFS, OTSM and the blockwise implementation as well as the interpolation pilot-based channel estimation method. In MIMO OTFS and OTSM simulations, the blockwise implementation is adopted.

4.2.1 Multiple Pilots Channel Estimation Method

In this simulation, we place the pilot on delay index 58 and Doppler index 0 on the

doi:10.6342/NTU202503398

DD grid with the guard symbol length 6 rows at transmitter A, and place the pilot on delay index 61 and Doppler index 0 on the DD grid with the guard symbol length 6 rows at transmitter B. The other parameters are the same as the previous chapters. The BER and NMSE performance at given speeds are shown in Figure 4.8 and Figure 4.9. The NMSE, used to evaluate the accuracy of channel estimation, is defined as:

$$NMSE = \left\|\hat{G} - G\right\|_F / \|G\|_F. \tag{4.2}$$

, where $\hat{G}, G$ denote the estimated channel and the real channel, while $\|\cdot\|$ represent the Frobenius norm.

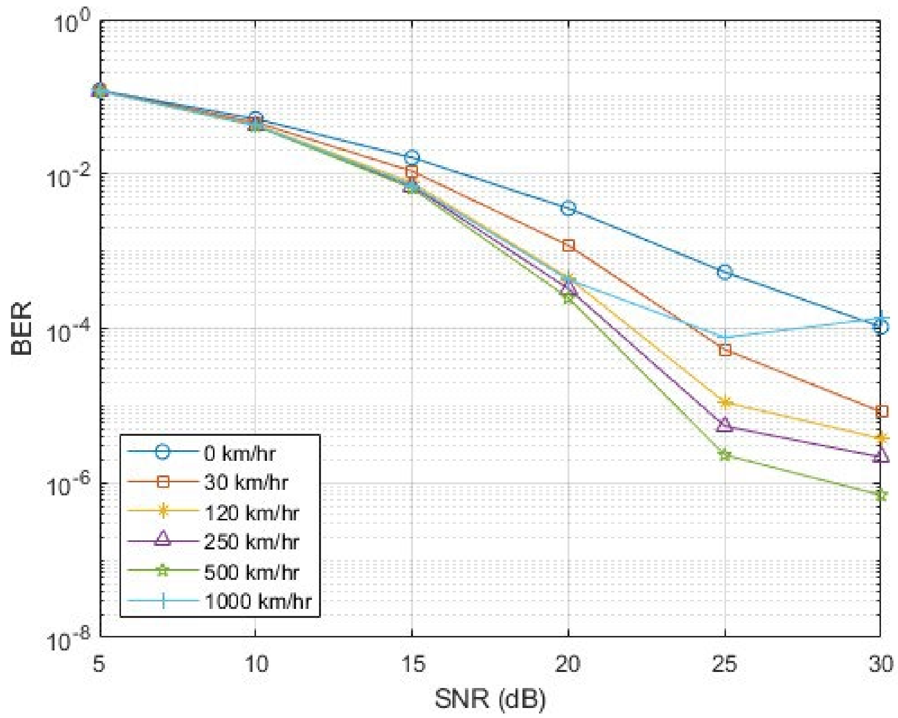

Figure 4.8 BER of MIMO OTFS/OTSM with Multiple Pilots Channel Estimation

doi:10.6342/NTU202503398

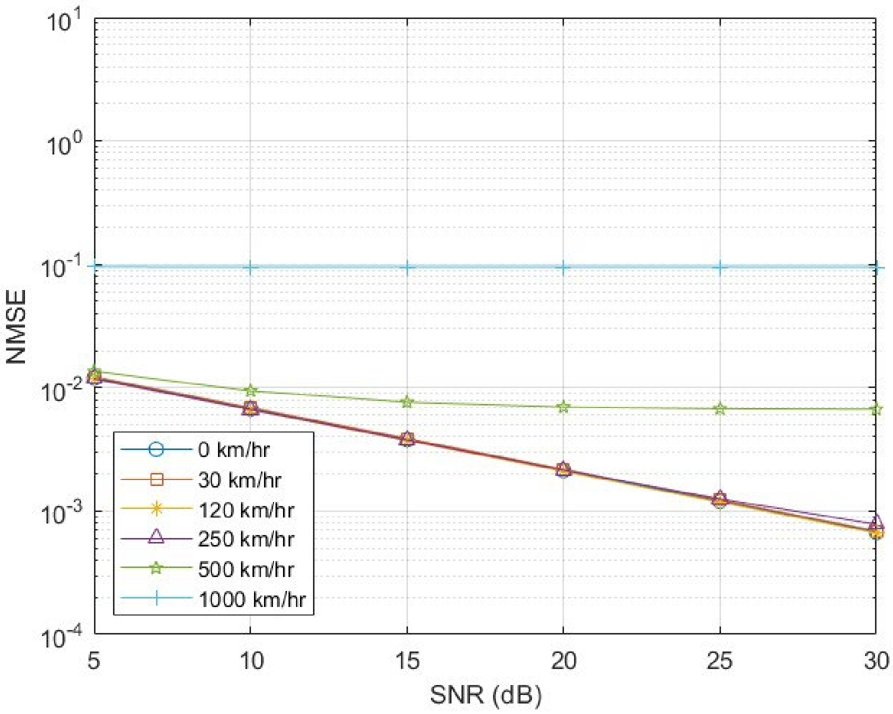

Figure 4.9 NMSE of MIMO OTFS/OTSM with Multiple Pilots Channel Estimation

The simulations show that BER and NMSE performances are satisfactory at lower speeds (e.g., 250 km/h or below), and remain acceptable at higher speeds (e.g., 500 km/h or above), albeit at the cost of increased guard symbol overhead.

However, allocating separate guard symbols reduces effective data throughput, which may be critical in bandwidth-limited scenarios.

4.2.2 Proposed Channel Estimation Method

In this simulation, we place the pilot on delay index 61 and Doppler index 0 on the DD grid with the guard symbol length 3 rows, the other parameters are the same as the previous chapters. The BER and NMSE performance of the first-ordered channel estimation method at given speeds are shown in Figure 4.10 and Figure 4.11.

doi:10.6342/NTU202503398

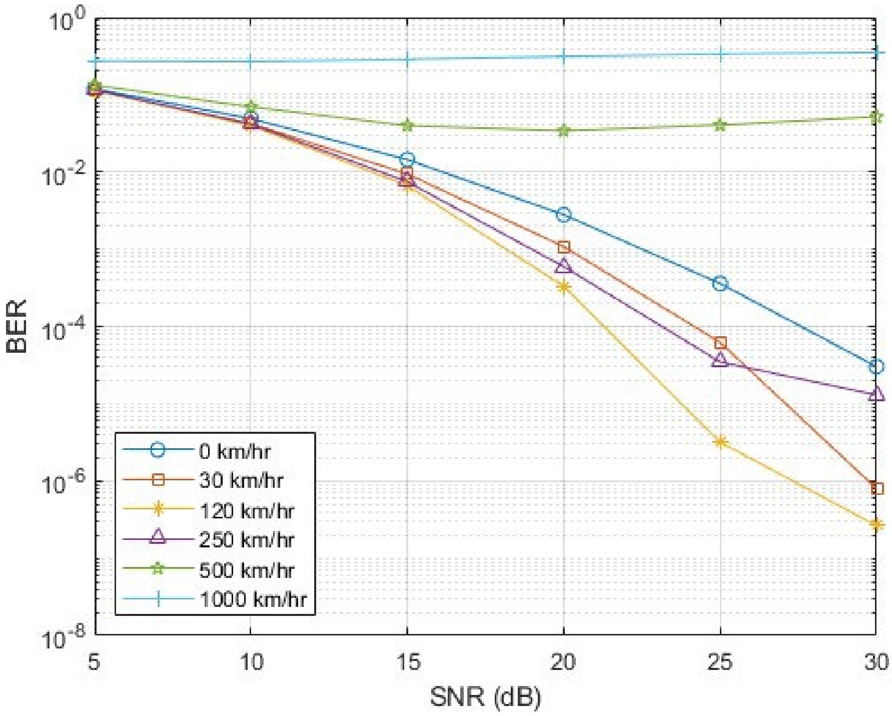

Figure 4.10 BER of MIMO OTFS/OTSM with First-Order Channel Estimation

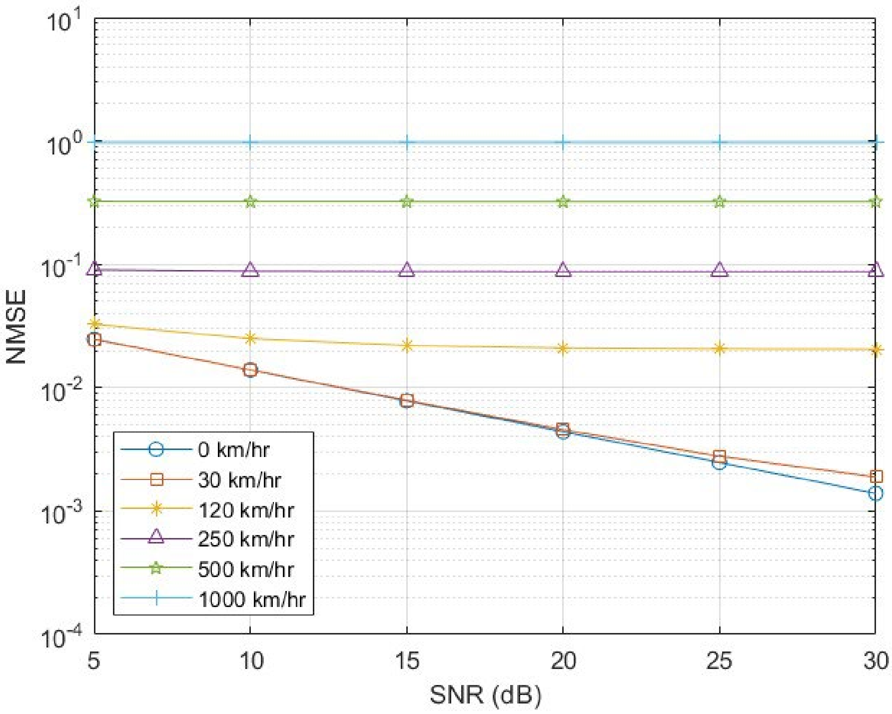

Figure 4.11 NMSE of MIMO OTFS/OTSM with First-Order Channel Estimation

doi:10.6342/NTU202503398

From the figures, we can find out that the first-order channel estimation method demonstrates poor performance. At the speed of 120 km/hr and higher, the NMSE values will not decrease as the SNR values increase, which is not applicable for high-speed situations.

The second-order channel estimation method is not applicable when $M = N = 64$, as 64 is not divisible by 6. Therefore, this method is applied with modifications.

The BER and NMSE performance of the third-ordered channel estimation method at given speeds are shown in Figure 4.12 and Figure 4.13.

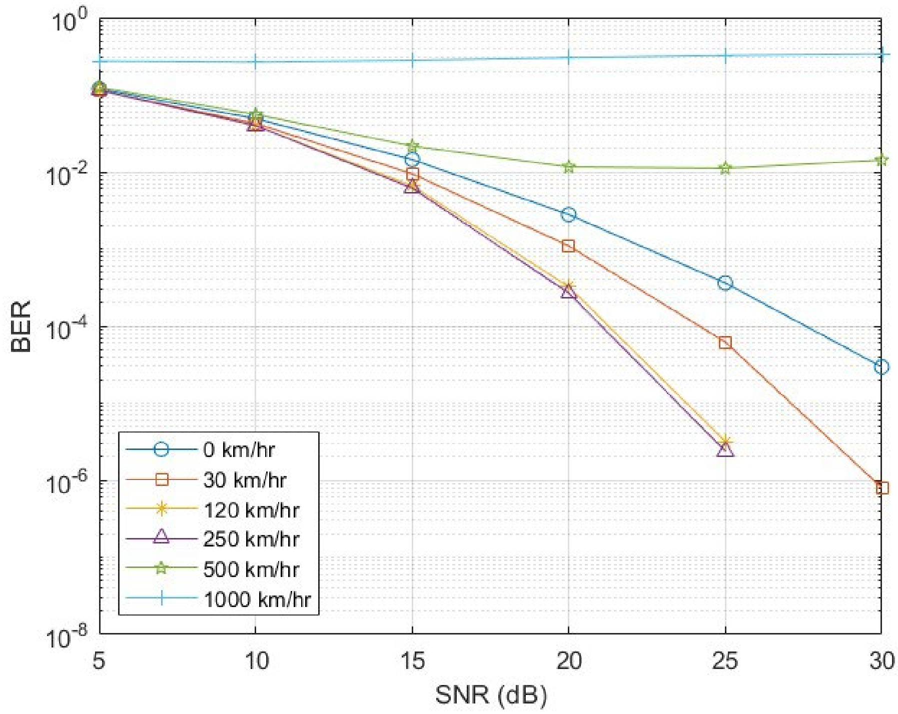

Figure 4.12 BER of MIMO OTFS/OTSM with Third-Order Channel Estimation

doi:10.6342/NTU202503398

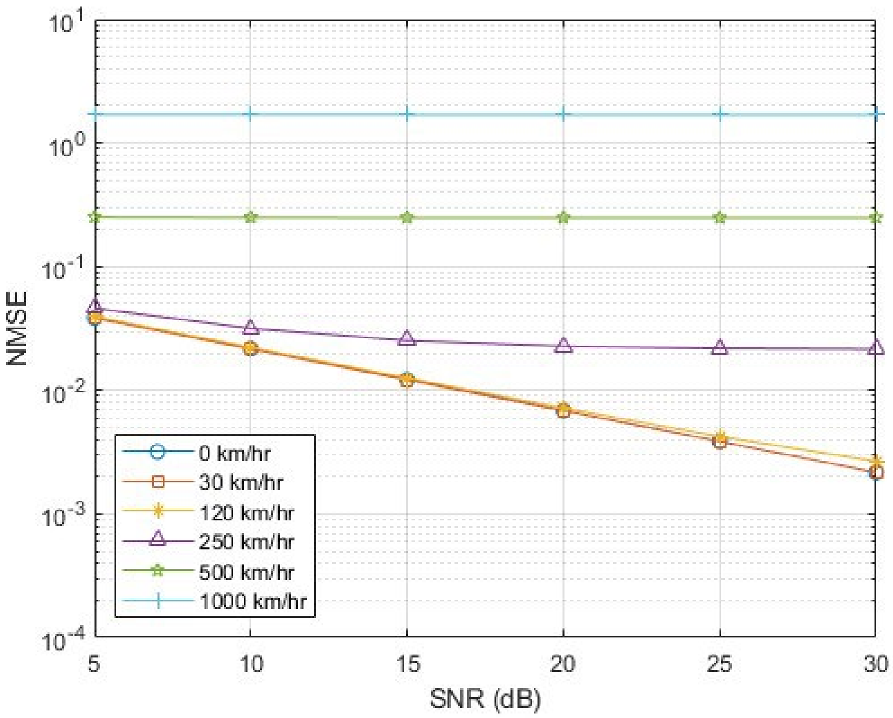

Figure 4.13 NMSE of MIMO OTFS/OTSM with Third-Order Channel Estimation

Simulations reveal that the third-order channel estimation method outperforms the first-order method in terms of BER and NMSE at speeds below 250 km/h; however, its performance remains inadequate at speeds of 500 km/h or higher.

We compare the modifications of the second-ordered channel estimation method with the third-ordered channel estimation method, find out that the performance of second-ordered channel estimation method is better than the third-ordered channel estimation method. Here, we show the BER and NMSE performance of the modifications of the second-ordered channel estimation method in Figure 4.14 to Figure 4.19.

doi:10.6342/NTU202503398

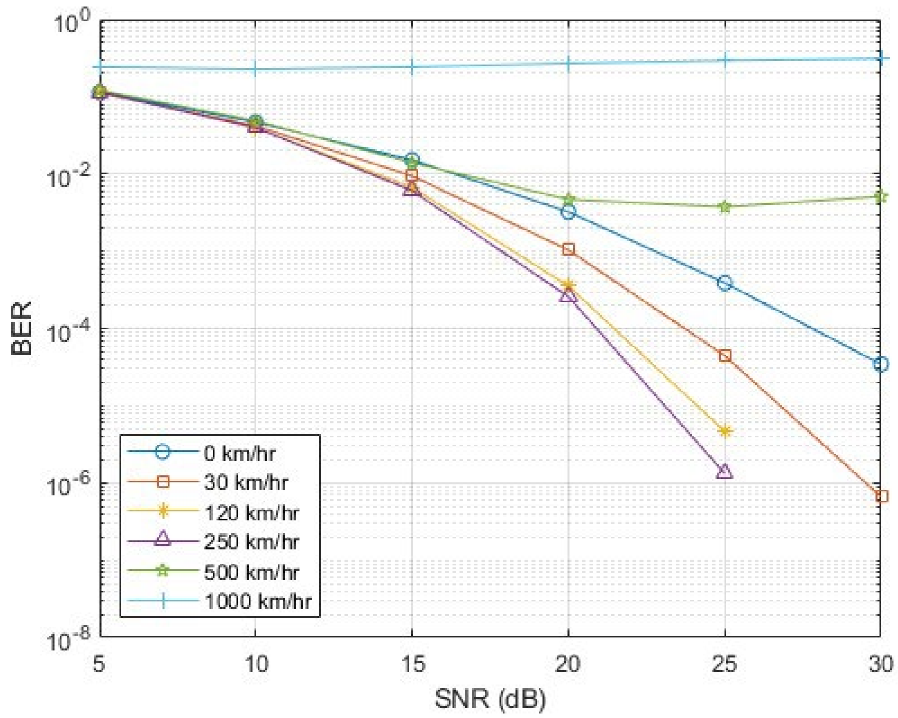

Figure 4.14 BER of MIMO OTFS/OTSM with Second-Order Channel Estimation

(Modification 1)

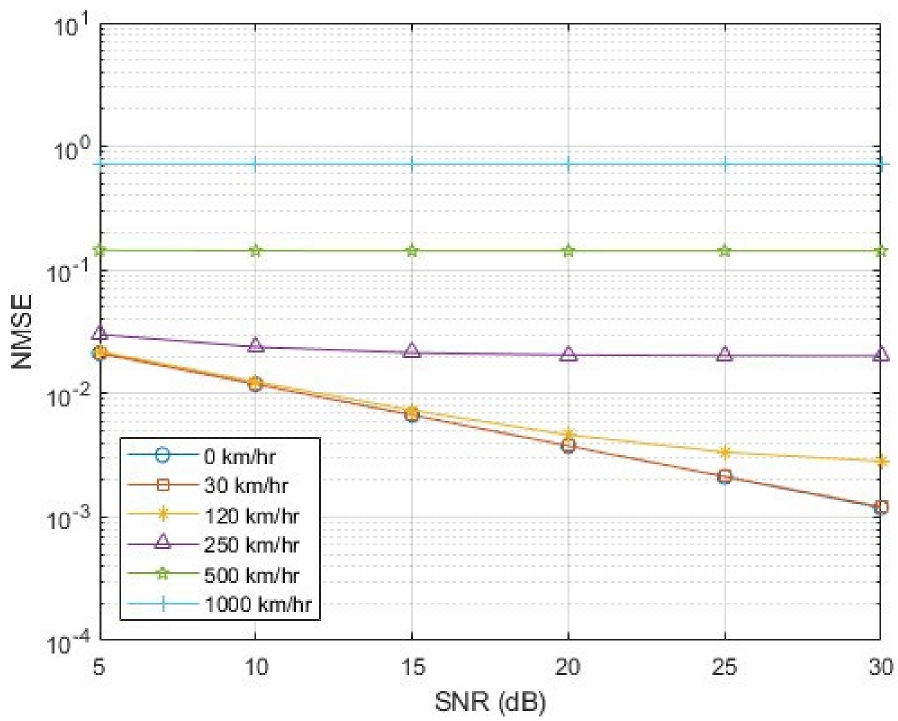

Figure 4.15 NMSE of MIMO OTFS/OTSM with Second-Order Channel Estimation

(Modification 1)

doi:10.6342/NTU202503398

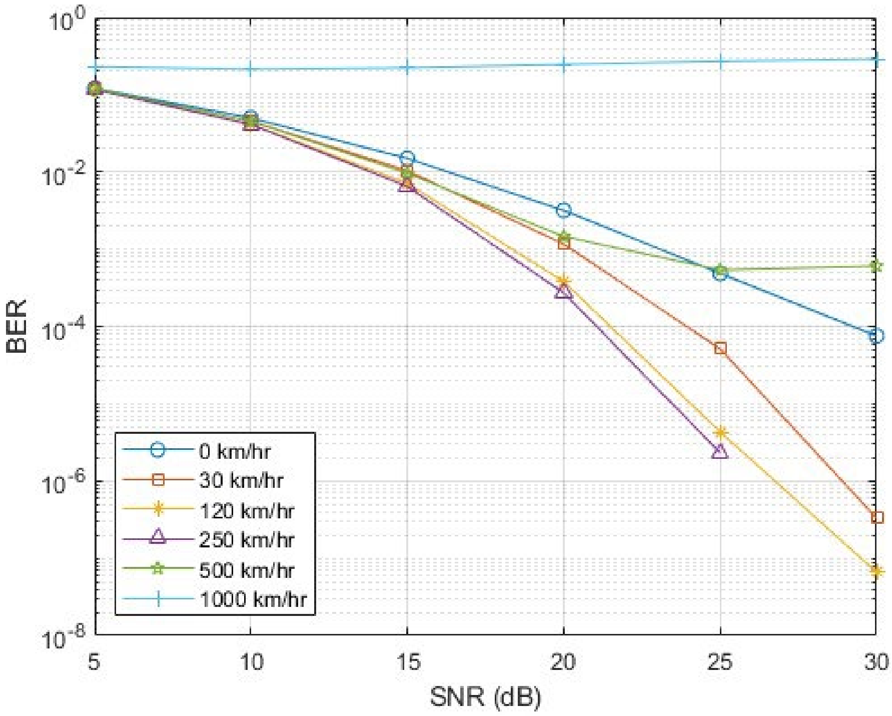

Figure 4.16 BER of MIMO OTFS/OTSM with Second-Order Channel Estimation

(Modification 2)

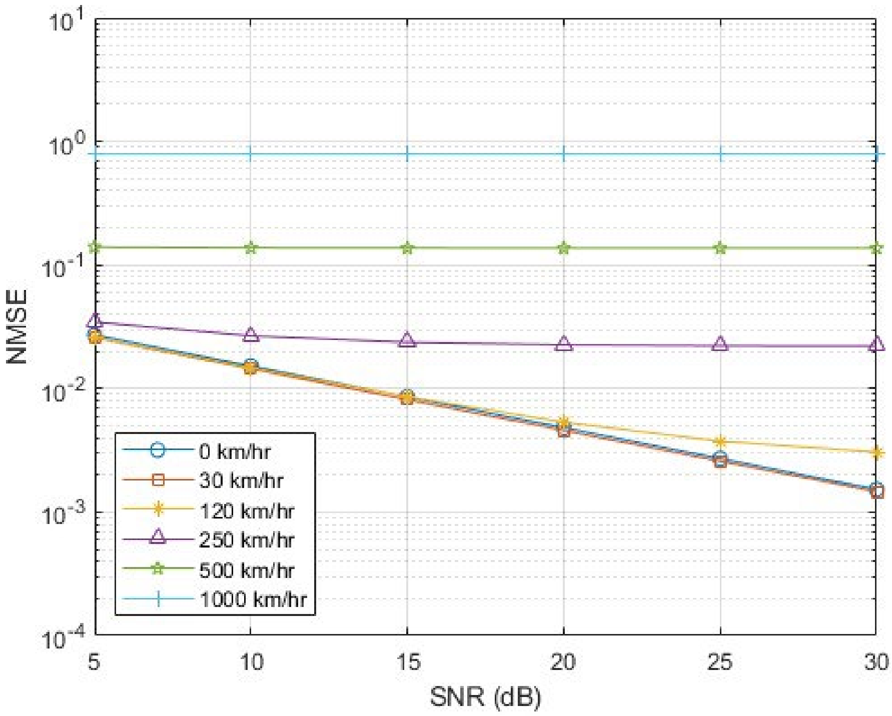

Figure 4.17 NMSE of MIMO OTFS/OTSM with Second-Order Channel Estimation

(Modification 2)

doi:10.6342/NTU202503398

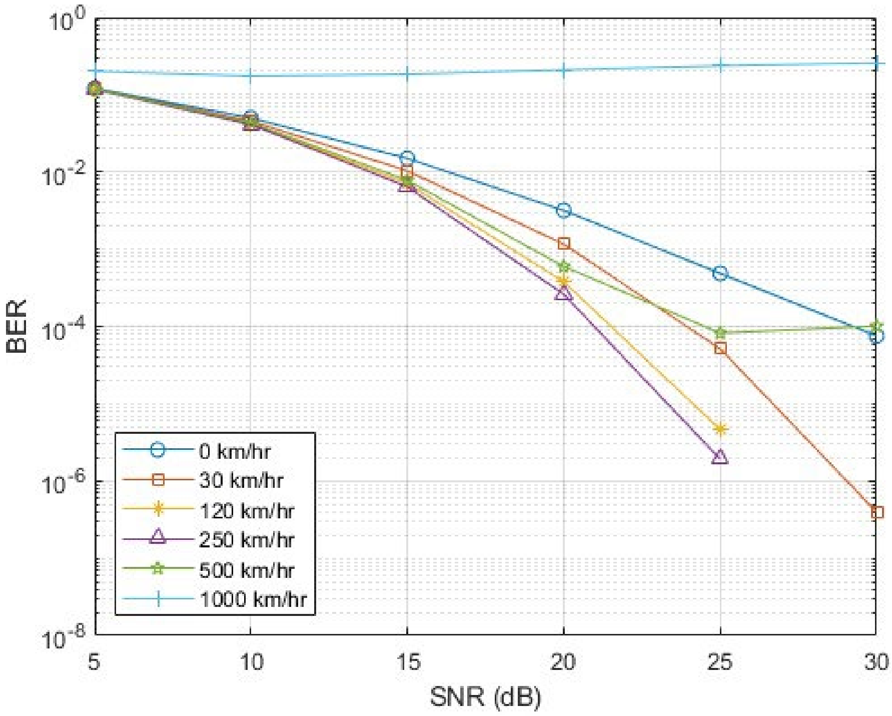

Figure 4.18 BER of MIMO OTFS/OTSM with Second-Order Channel Estimation

(Modification 3)

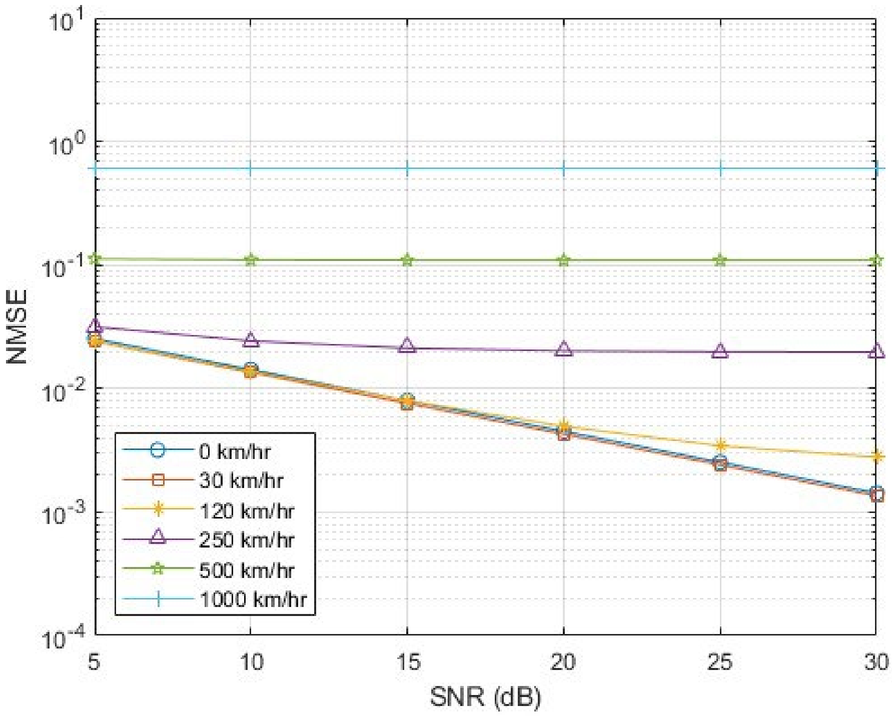

Figure 4.19 NMSE of MIMO OTFS/OTSM with Second-Order Channel Estimation

(Modification 3)

doi:10.6342/NTU202503398

Among the tested modifications, Modification 3 yields the best performance for the second-order channel estimation method — delivering good results at speeds below 250 km/h and acceptable performance at 500 km/h.

In conclusion, the proposed method effectively reduces overhead in MIMO OTFS and OTSM systems, maintaining comparable BER and NMSE performance at low speeds, but exhibiting poor performance in extreme high-speed scenarios.

4.3 Summary

This chapter presented extensive simulations under the 3GPP EVA channel to validate the proposed methods. In SISO tests, OTFS and OTSM showed nearly identical BER performance across speeds up to 1000 km/h, with blockwise MMSE matching full-frame MMSE at far lower complexity.

Pilot-based interpolation achieved low NMSE using either linear or spline reconstruction. In MIMO evaluations, the multi-pilot baseline delivered good accuracy but at heavy overhead.

The proposed single-pilot method closely matched baseline BER and NMSE at low speeds ($\leq$ 250 km/h) and—with the three modifications—outperformed it at very high speeds ($\geq$ 500 km/h), demonstrating that polynomial-based, sign-alternating channel estimation can yield both pilot efficiency and robust performance in rapidly time-varying MIMO channels.

doi:10.6342/NTU202503398

第五章　Conclusion and Future Work

5.1　Conclusion

In this thesis, we have investigated the channel estimation and equalization techniques for OTFS and OTSM systems, with a particular focus on high-mobility scenarios. The blockwise MMSE equalization scheme effectively reduces computational complexity while maintaining comparable detection performance to conventional MMSE methods.

For channel estimation, a pilot-assisted interpolation method was developed for both SISO and MIMO systems. In the SISO case, interpolation-based estimation combined with proper pilot placement achieves reliable performance even in rapidly varying channels.

In the MIMO scenario, we addressed the challenge of pilot contamination by proposing a novel channel estimation method using structured pilot design and polynomial curve fitting. Furthermore, we examined several refinement strategies to mitigate estimation errors in high Doppler environments, demonstrating improved NMSE and BER performance in simulation results.

Overall, the proposed method offer a practical trade-off between estimation accuracy and pilot overhead, particularly under low to moderate mobility conditions.

5.2　Future Work

Although the proposed methods achieve promising results, several aspects remain open for future research:

1. Extension to Higher-Order MIMO Systems:

   The current study focuses on 2×2 MIMO systems. Extending the proposed channel

doi:10.6342/NTU202503398

estimation methods to larger MIMO configurations (e.g., massive MIMO) requires addressing increased pilot contamination and complexity.

2. Adaptive Curve Fitting for Dynamic Channels:

The current fitting methods use fixed-order polynomials. Future work may explore adaptive curve fitting techniques or machine learning-based approaches to dynamically adjust the fitting strategy based on real-time channel characteristics.

doi:10.6342/NTU202503398

參考文獻

[1] R. Hadani et al., "Orthogonal Time Frequency Space Modulation," 2017 IEEE Wireless Communications and Networking Conference (WCNC), San Francisco, CA, USA, 2017, pp. 1-6, doi: 10.1109/WCNC.2017.7925924.

[2] P. Raviteja, Y. Hong, E. Viterbo and E. Biglieri, "Practical Pulse-Shaping Waveforms for Reduced-Cyclic-Prefix OTFS," in IEEE Transactions on Vehicular Technology, vol. 68, no. 1, pp. 957-961, Jan. 2019, doi: 10.1109/TVT.2018.2878891.

[3] T. Thaj and E. Viterbo, "Orthogonal Time Sequency Multiplexing Modulation," 2021 IEEE Wireless Communications and Networking Conference (WCNC), Nanjing, China, 2021, pp. 1-7, doi: 10.1109/WCNC49053.2021.9417451.

[4] T. Thaj, E. Viterbo and Y. Hong, "Orthogonal Time Sequency Multiplexing Modulation: Analysis and Low-Complexity Receiver Design," in IEEE Transactions on Wireless Communications, vol. 20, no. 12, pp. 7842-7855, Dec. 2021, doi: 10.1109/TWC.2021.3088479.

[5] S. G. Neelam and P. R. Sahu, "Detection Techniques for SISO/MIMO-OTSM Systems with Hardware Impairments Under High Mobility Scenarios," 2024 National Conference on Communications (NCC), Chennai, India, 2024, pp. 1-6, doi: 10.1109/NCC60321.2024.10485695.

[6] H. F. Harmuth, "Applications of Walsh functions in communications," in IEEE Spectrum, vol. 6, no. 11, pp. 82-91, Nov. 1969, doi: 10.1109/MSPEC.1969.5214175.

[7] F. Lampel, A. Avarado and F. M. J. Willems, "On OTFS using the Discrete Zak Transform," 2022 IEEE International Conference on Communications Workshops (ICC Workshops), Seoul, Korea, Republic of, 2022, pp. 729-734, doi:

doi:10.6342/NTU202503398

10.1109/ICCWorkshops53468.2022.9814589.

[8] K. R. Murali and A. Chockalingam, "On OTFS Modulation for High-Doppler Fading Channels," 2018 Information Theory and Applications Workshop (ITA), San Diego, CA, USA, 2018, pp. 1-10, doi: 10.1109/ITA.2018.8503182.

[9] P. Raviteja, K. T. Phan, Y. Hong and E. Viterbo, "Embedded Delay-Doppler Channel Estimation for Orthogonal Time Frequency Space Modulation," 2018 IEEE 88th Vehicular Technology Conference (VTC-Fall), Chicago, IL, USA, 2018, pp. 1-5, doi: 10.1109/VTCFall.2018.8690836.

[10] B. Zhu and Z. Luo, "A High-Performance Block LMMSE Equalizer for OTFS-MIMO Diversity and Multiplexing," 2022 IEEE 8th International Conference on Computer and Communications (ICCC), Chengdu, China, 2022, pp. 928-932, doi: 10.1109/ICCC56324.2022.10065865.

[11] X. Huang, A. Farhang and R. -R. Chen, "Channel Estimation and Turbo Equalization for Coded OTFS and OFDM: A Comparison," in IEEE Wireless Communications Letters, vol. 12, no. 9, pp. 1613-1617, Sept. 2023, doi: 10.1109/LWC.2023.3284778.

[12] S. S. Das, V. Rangamgari, S. Tiwari and S. C. Mondal, "Time Domain Channel Estimation and Equalization of CP-OTFS Under Multiple Fractional Dopplers and Residual Synchronization Errors," in IEEE Access, vol. 9, pp. 10561-10576, 2021, doi: 10.1109/ACCESS.2020.3046487.

[13] S. Sabapathy, J. S. Prabhu, S. Maruthu and D. N. K. Jayakody, "Profuse Channel Estimation and Signal Detection Techniques for Orthogonal Time Frequency Space in 6G Epoch: A Survey," in IEEE Access, vol. 11, pp. 129963-129993, 2023, doi: 10.1109/ACCESS.2023.3333428.

[14] T. Thaj and E. Viterbo, "Low Complexity Iterative Rake Decision Feedback

doi:10.6342/NTU202503398

Equalizer for Zero-Padded OTFS Systems," in IEEE Transactions on Vehicular Technology, vol. 69, no. 12, pp. 15606-15622, Dec. 2020, doi: 10.1109/TVT.2020.3044276.

[15] T. Thaj and E. Viterbo, "Low Complexity Iterative Rake Detector for Orthogonal Time Frequency Space Modulation," 2020 IEEE Wireless Communications and Networking Conference (WCNC), Seoul, Korea (South), 2020, pp. 1-6, doi: 10.1109/WCNC45663.2020.9120526.

[16] P. Raviteja, K. T. Phan, Y. Hong and E. Viterbo, "Interference Cancellation and Iterative Detection for Orthogonal Time Frequency Space Modulation," in IEEE Transactions on Wireless Communications, vol. 17, no. 10, pp. 6501-6515, Oct. 2018, doi: 10.1109/TWC.2018.2860011.

[17] 3GPP TS 36.101. "Evolved Universal Terrestrial Radio Access (E-UTRA); User Equipment (UE) Radio Transmission and Reception," 3rd Generation Partnership Project; Technical Specification Group Radio Access Network.

[18] de Boor, Carl, A Practical Guide to Splines. Springer-Verlag, New York: 1978.

doi:10.6342/NTU202503398